RSC Chemical Biology

ROYAL SOCIETY OF CHEMISTRY

REVIEW

Cite this: *RSC Chem. Biol.*, 2022, 3, 830

Protein scaffolds: antibody alternatives for cancer diagnosis and therapy

Renli Luo, [a] Hongguang Liu *[a] and Zhen Cheng *[bc]

Received 5th April 2022,
Accepted 23rd May 2022

DOI: 10.1039/d2cb00094f

rsc.li/rsc-chembio

Although antibodies are well developed and widely used in cancer therapy and diagnostic fields, some defects remain, such as poor tissue penetration, long *in vivo* metabolic retention, potential cytotoxicity, patent limitation, and high production cost. These issues have led scientists to explore and develop novel antibody alternatives. Protein scaffolds are small monomeric proteins with stable tertiary structures and mutable residues, which emerged in the 1990s. By combining robust gene engineering and phage display techniques, libraries with sufficient diversity could be established for target binding scaffold selection. Given the properties of small size, high affinity, and excellent specificity and stability, protein scaffolds have been applied in basic research, and preclinical and clinical fields over the past two decades. To date, more than 20 types of protein scaffolds have been developed, with the most frequently used being affibody, adnectin, ANTICALIN®, DARPins, and knottin. In this review, we focus on the protein scaffold applications in cancer therapy and diagnosis in the last 5 years, and discuss the pros and cons, and strategies of optimization and design.

Introduction

Cancer is a severe disease that threatens human health. Traditional cancer treatments were designed as one-size-fits-all approaches; however, not all patients benefited from the same method owing to inter- and intra-tumor heterogeneity between individuals.[1] To deal with these issues, precision medicine using multi-omics information analyses has been proposed to identify the crucial tumor markers for classifying patients and tailoring precisely targeted treatments.[2–4]

Monoclonal antibodies against tumor markers are the most widely investigated targeting elements for precise cancer diagnosis and treatment.[5,6] Generally, antibodies are large size proteins, which comprise two pairs of heavy and light chains that form a stable Y-shape structure *via* disulfide bond linking. Antibodies can recognize biomarkers on cell surfaces, thereby activating immune responses or suppressing protumoral biological activities.[7,8] However, several defects deter the further application of antibodies. For instance, the large molecular weight leads to poor tissue penetration for solid tumors, and hinders the binding of inside antigenic epitopes and the internalization of antibody-conjugated drugs.[9] Posttranslational modifications are indispensable in facilitating the production of antibodies with complete functionality; however, these require the use of a high-cost and time-consuming eukaryotic expression system, which limits the large-scale production and access to most patients.[10] Moreover, it may be difficult to introduce free residues and chemical linkers for further drug conjugation. In addition, in some situations, the antibody constant fragment (Fc) might incur immune-related cytotoxicity, resulting in damage to normal tissues and organs.[11] While truncated antibodies such as antigen-binding fragments (Fab/scFvs) and alpaca nanobodies have been developed to remedy the shortcomings of full-size antibodies, some defects remained, such as lower avidity after modification and the requirement of humanization processing for reducing immunogenicity.[12,13]

Hence, urgent demands for addressing these limitations have motivated scientists to explore novel antibody alternatives. Based on the discoveries of small molecule proteins with binding function and the gradual development of biotechnology, it is feasible to confer targeting ability to small size proteins by mutating the variable region.[14] Technically, a protein scaffold (Fig. 1)† is a small single-domain molecule (1–20 kDa),

[a] *Department of Molecular Medicine, College of Life and Health Sciences, Northeastern University, Shenyang, China. E-mail: simonliu@mail.neu.edu.cn*
[b] *State Key Laboratory of Drug Research, Molecular Imaging Center, Shanghai Institute of Materia Medica, Chinese Academy of Sciences, Shanghai, 201203, China. E-mail: zcheng@simm.ac.cn*
[c] *Drug Discovery Shandong Laboratory, Bohai Rim Advanced Research Institute for Drug Discovery, Yantai, Shandong 264117, China*

† Crystal structures for the protein scaffolds shown in Fig. 1 were obtained from the PDB (https://www.rcsb.org/): (A) affibody (PDB ID: 3MZW);[207] (B) ANTICALIN® (PDB ID: 4GH7);[208] (C) adnectin or Monobody (PDB ID: 1TTG);[209] (D) Knottin (PDB ID: 2IT7);[210] (E) designed ankyrin repeat proteins (PDB ID: 1MJ0);[211] (F) nanofitin or affitin (PDB ID: 4CJ2);[212] (G) centyrins (PDB ID: 5L2H);[213] (H) Kunitz (PDB ID: 1KTH);[214] (I) affimer (PDB ID: 1NB5);[215] (J) avimer (PDB ID: 1AJJ);[216] (K) affilin based on the ubiquitin (PDB ID: 1UBI);[217] and (L) affilin based on the γ-B-crystalin (PDB ID: 2JDG).[218]

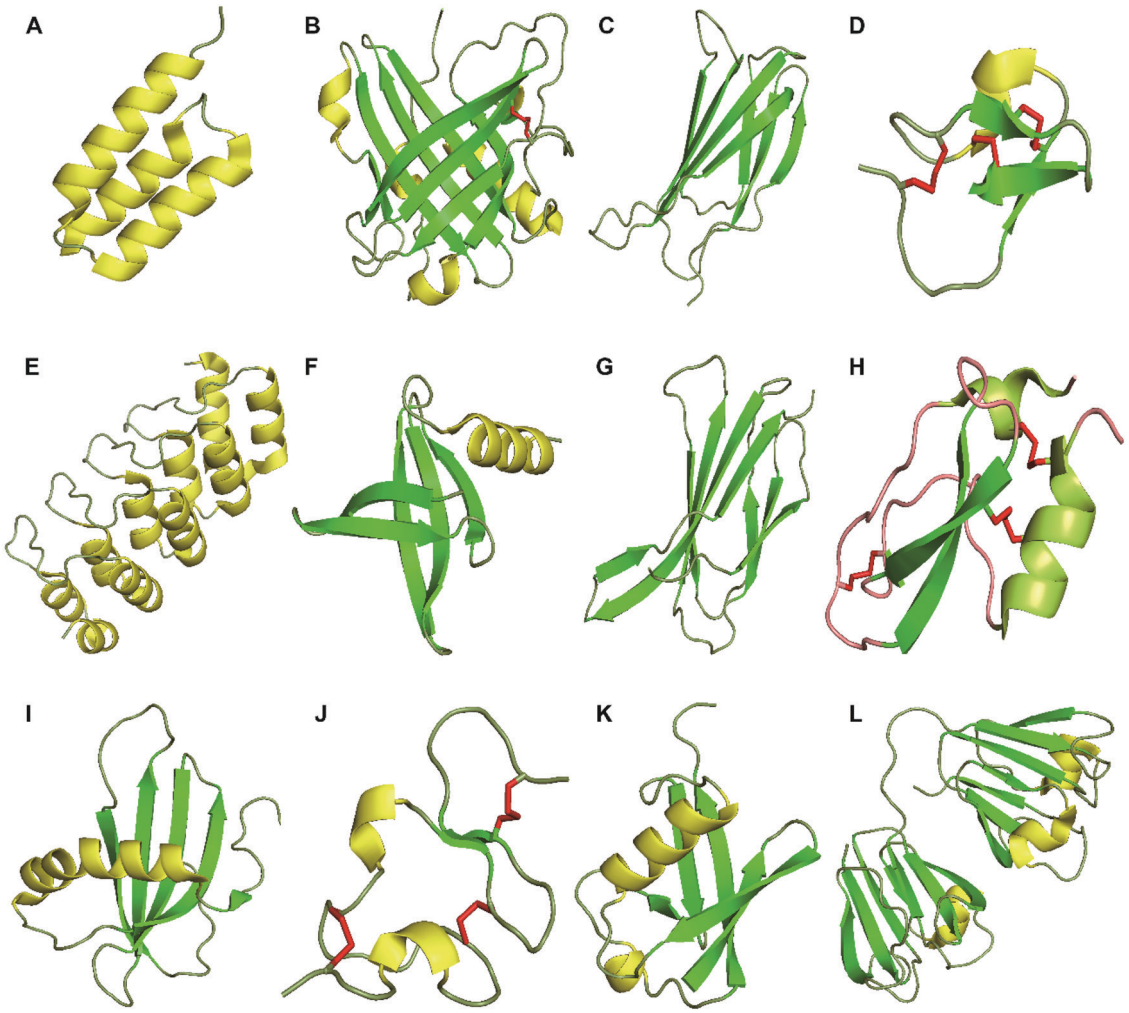

Fig. 1 Structures of proteins scaffolds. Notes: cartoon-illustrations are generated using PyMol, β-sheets are shown in green, α-helix structures are displayed in yellow and disulfide bonds are colored in red. (A) Affibody (PDB ID:3MZW); (B) ANTICALIN® (PDB ID: 4GH7); (C) adnectin or monobody (PDB ID: 1TTG); (D) Knottin (PDB ID: 2IT7); (E) designed ankyrin repeat proteins (PDB ID: 1MJ0); (F) Nanofitin or Affitin (PDB ID: 4CJ2); (G) centyrins (PDB ID: 5L2H); (H) Kunitz (PDB ID: 1KTH); (I) affimer (PDB ID: 1NB5); (J) avimer (PDB ID:1AJJ); (K) Affilin based on the ubiquitin (PDB ID:1UBI); and (L) affilin based on the γ-B-crystalin (PDB ID: 2JDG).

composed of two parts, which are analogous to antibodies. The first component is the constant region, which comprises a couple of α-helixes or beta-sheets constituting a rigid tertiary structure, while the second is the variable region, which is formed by a few exposed loops or several residues in the rigid secondary structures. The constant regions sustain inherent conformational stability of protein scaffolds, and variable sites provide a specific binding capability to various target molecules *via* structural ligand–receptor pairing or chemical forces. Generally, 10–20 amino acid residues in the protruded loops or rigid structures can be randomized to obtain novel affinity molecules. Protein scaffolds often lack disulfide bonds and require no translational modifications, allowing production using cost-effective prokaryotic expression systems. Furthermore, unnatural and free residues can be introduced into protein scaffolds *via* chemical synthesis for drug or diagnostic reagent conjugation. Small protein scaffolds are usually soluble with good physicochemical stability which favors their *in vivo* application.[9,15]

Despite the many advantages of protein scaffolds, they are more suitable for short-term cancer imaging, not therapy. Table 1 summarizes the major properties and developed targets of protein scaffolds.

Conjugation strategies for protein scaffolds

Conjugating proteins with diagnostic or therapeutic compounds is necessary for functional probes or nanomedicine preparation.[16,17]

Generally, there are four ways to realize bioconjugation. Cysteine-based conjugation uses the thiol group within free cysteine to react with maleimide or iodoacetamide-modified compounds and form stable covalent bonds.[18] Besides, reporters or drugs can be directly conjugated to the disulfide bonds using next-generation maleimides.[19] Lysine-based conjugation is built

Table 1 The overview of protein scaffolds properties and molecular targets

Protein scaffolds	Parental protein	Molecular size (kDa)	Affinity (K_d)	Structural feature	Targets
Affibody	B-domain of *staphylococcal* protein A	6.5	μM–pM	α-Helix	RSV-G protein, Taq DNA polymerase, human factor VIII, human IgA, Staphylococcal protein A domain, apolipoprotein A1, CD28, GP120, transferrin, CD25, c-Jun, H-Ras, Raf-1, VEGFR, HER2, murine lgG1, insulin, IAPP, IL-6, Tau, IGF1R, Aβ, TNF-α, IL-17, VEGFR-2, LOV, HER3, C5, CAIX, PDGFRβ, PD-L1, FcRn, HPV16 E7, EGFR, CTX-M15, CD276, EBV-LMP-2, fibrinogen, IgE, IgM, IL-1, IL-8, HAS, transthyretin
ANTICALIN®	Lipocalin	18–20	nM–pM	β-Barrel and terminal α-helix	Fluorescein, digoxigenin, hemoglobin, nonsymmetric phthalic acid ester, CTLA-4-Fc, estradiol-2, MET, hepcidin, VEGF-A, fibronectin extra-domain B, CD137, IL4Rα, PSMA, Aβ peptide, VEGFR-3, monosaccharide, HSP70, PCSK9, petrobactin, colchicine, CD98, IL-17, IL-23
Adnecin/ monobody	10th type III domain of human fibronectin	10	μM–pM	β-Sandwich	Ubiquitin, estrogen receptor α, leptin, TNF-α, αvβ3 integrin, c-Src, VEGFR-2, hen egg-white lysozyme, MBP, hSUMO4, phosphor-IκBα, SARS-N protein, Abl kinase SH2 domain, EGFR, IGF-1R, IL-6, Fyn-SH3 domain, human IgG, Pak1 kinase, IL-23, Erk-2 CD domain, SHP2 SH2 domains, GFP, PCSK9, hEphA2, β-galactosidase, CDC34, COPS5, MAP2K5, SF3A1, USP11, human pregnane X receptor, KEAP1, GPR56, myostatin, H-Ras, CD4, C258S, methyltransferase, mesothelin, Candida rugosa lipase 1, MAPK, WDR5, PD-L1, gp41, glypican-3, VEGFR2, CD80, oncoprotein aurora A kinase, SET, Bcr-Abl p210, MLKL N-terminal domain
DARPins	Human ankyrin repeat proteins	14–21	nM–pM	α-Helix and β-turn	MBP, JNK2 kinase, NIa(pro) proteinase, AcrB, Na^+ citrate symporter, caspase-2, apo Plk-1, CD4, TNF-α, EGFR, HER2, HER4, human IgG-Fc, IgE, neurotensin receptor 1, FcεRIα, EpCAM, NEMO-CC2-LZ, BCL-2, adenoviruses fiber protein knob domain, MsbA, JNK, LmrCD, tubulin, ERK2, BCL-W, VEGF-A, caspase-3, gp120, antigen FVIII, PDGF-BB, BCL-XL, caspase-7, human telomere quadruplex, Aβ, GFP, IL-4, CDCP1, lamin A/C, CD23, tubulin, MCL-1, IL-13, ribosomal protein S6 kinase 2, FccRIIB, K-Ras, cathepsin B, HSA, GluA4, CD105, NKp46, TNFR2, mTFP1, MET, EpoR, TcdB, ESAT-6, listeriolysin O, CD8, HER3, VEGF, HGF, CD137, CD40, fibroblast activation protein, Wnt enhanceosome ChiLS, CD8, KRAS
Knottin	Cystine kont from agatoxin, chlorotoxin, EETI, kalata B1, MCoTI-I/II, SOTI, AgRP	<4	Sub-nM–nM	β-Strands and 3 S–S formed macrocycle	Matrix metalloproteinase-2, thrombopoietin, FMDV-3C protease, VEGF-A, human thrombopoietin receptor, β-tryptase, NS2B–NS3 protease, MC4R, CXCR4, neuropilin-1, neuropilin-2, human matriptase-1, Hdm2/X, CTLA-4, BCR-ABL, α-synuclein, thrombospondin-1, SET protein, factor XIIa, angiotensin, IL-10, ebvIL-10, human fibronectin ED-B domain, αvβ3, αvβ5, α5β1, α(IIb)β(3), α9β1,α4β1, αvβ6 integrin
Kunitz	Serine protease inhibitor from BPTI/APPI/ TFPI	7	nM–pM	α-Helix, β-sheet and 3 S–S	Human plasma kallikrein, mesotrypsin, KLK-related peptidase 6, factor VIIa (TF-FVIIa), factor X (FXa), thrombin, IL-6R, human plasmin, neutrophil elastase, matriptase-2, Rho-GTPases, uPA receptor
Affimer	Human stefin A protease inhibitor	11	μM–nM	α-Helix, β-strands	CDK2,Src-Homology 2 (SH2) domains, CRP, SUMO, VEGFR2, HER4, AGR2, TRPV1 ion channel, PEDF, tenascin C, GFP, osteonectin, HTV-derived protein UL49, NS1 protein, tubulin, Myc, CDK4, PI-3K-P85 subunit, PD-L1 and LAG-3
Nanofitin/ affitin	DNA binding protein Sac7d	7	μM–sub-nM	β-Barrel capped with an α-helix	Human IgG, EGFR, GFP, PulD protein, hrEpCAM, chicken egg lysozyme, staphylococcal protein A, thermophilic CelD
Avimer	A-domain of cell membrane receptors (LRP,VLDLR)	4	Sub-nM	β-Strands and 3 S-S	IL-6, endocrine hormone FGF21, MET, human type II collagen, BAFF
Centyrins	Fn III domain human tenascin C	10	nM–pM	β-Sheet	C-MET, FcγRIIB, murine IL-17A EGFR, *S. aureus* leukocidins, rat TNFα
Affilin	Human γ-B-crystallin Ubiquitin	20 10	μM–pM	β-Sheet α/β	HER2, human IgG-Fc, EGFR, fibronectin ED-B domain, human proNGF protein, human papillomavirus E7 protein, estradiol/testosterone
ADAPT	Albumin-binding domain	5	Sub-nM–nM	α-Helix	HER2, HER3, IL-23, IL-17, hIFNγ, TNF-α

upon the good nucleophilicity of the reactive amine side chain from the solvent-accessible lysine. Normally, *N*-hydroxysuccinimidyl (NHS)- or sulfo-NHS ester-modified compounds react with the amine group of lysines to produce amide or amidine bonds,[20] and unnatural amino acid (UAA)-based biorthogonal reaction and enzymatic conjugation are also feasible.[21,22] For instance, 5-hydroxytryptophan (5 HTP) can be incorporated into specific sites of proteins *via* tryptophanyl-tRNA synthetase, following which compounds carrying aromatic diazonium groups quickly interact with 5 HTP *via* the azo-coupling reaction and realize conjugation.[23] Cycloaddition-conjugation using L-azidohomoalanine (Aha) has replaced the L-methionine of the protein in methionine-auxotrophic *E. coli* strains to generate stable triazole groups *via* azide amino acid reacting with the alkyne or dibenzocyclooctyne of payloads.[24] Photocrosslinking conjugation replaces the stop codon of protein with benzoylphenylalanine (BPA), while compounds with photoreactive antibody-binding domains (pAbBDs) can be conjugated with the BPA group under ultraviolet irradiation.[25] The enzymatic conjugation strategies take advantage of enzymes that selectively recognize and catalyze the protein-tag and compound interaction. Enzyme-recognition tag combinations, such as sortaseA-LPXTG tag, trypsiligase-YRH tag, *N*-myristoyltransferase-(M)GXXXS/TXXX tag, tubulin tyrosine ligase-tub tag, lipoic acid ligase-LAP tag, farnesyltransferase-C-terminal CaaX tag, and transglutaminase–glutamine–lysine, have also been applied for enzymatic conjugation.[26]

To date, cysteine-based conjugation remains the universal site-specific conjugation method for most protein scaffolds that have no cysteine, including affibody, centyrin, DARPins, and ADPTA. However, for cysteine-rich scaffolds such as knottin, kuntiz, ANTICALIN®, and avimer, thioether bond-based conjugation may result in inhomogeneous conjugates and disulfide scrambling of scaffolds without a proper re-oxidation environment. UAA and enzymatic catalysis are more appropriate conjugation approaches for disulfide bond-based scaffolds. *Via* the incorporation of an azide residue or a polypeptide-tag into the N-terminus, protein scaffolds can easily realize site-specific conjugation and produce homogeneous conjugates with little impact on the affinity and original structure. However, recognition tag sequence introduction and the slow reaction of cycloaddition-conjugation may be inevitable.

Affibody

The B domain of *Staphylococcal* protein A is the parental scaffold of the affibody (ABY) protein scaffold originally responsible for Fc binding of immunoglobulin G.[27] The B-domain contains 58 amino acid residues (6.5 kDa), constituting a three α-helix bundle motif without disulfide bonds. The B-domain was then artificially synthesized and denoted as the Z domain or affibody, which was used to construct a combinatorial library by randomizing 13 soluble surface residues located in the first two helixes.[28] In theory, a specific affibody against any given target can be selected *via* an affibody-display phage library. As the third helix contributes to the structural integrity of the affibody but not binding function, a 2-helix affibody was developed. Compensating stability with disulfide bridges or site mutation offered advantages including a smaller size, quicker clearance, and lower imaging background.[29] A homodimeric affibody ZAβ_3 has also been used against amyloid peptides to screen the aggregation inhibitor for Tau protein.[30] The Swedish company ''Affibody AB,'' founded in 1998, has explored affibodies and owns almost 300 patents.[31] Affibodies modified with imaging contrast agents, fluorescent labels, chemical drugs, and radiolabels have been applied in therapeutic and diagnostic cancer research.[32,33]

The anti-HER2 (human epidermal growth factor receptor 2) affibody is the most intensively investigated affibody thus far, with ABY-002($Z_{HER2:342}$) being the first to be applied in clinical computed tomography (CT) imaging for patients with breast cancer.[34] However, owing to its partial high hepatic accumulation, ABY-002 was optimized to improve its specificity, stability, and hydrophilicity to produce ABY-025. A clinical phase II study of ^{68}Ga-ABY-025 and ^{111}In-ABY-025 demonstrated rapid accumulation in the tumor site within 1 h and showed clearance from the kidneys. The imaging results provided the metastatic details of HER2-positive primary tumors for several patients (NCT01858116, NCT01216033) (Fig. 2).‡[35] A recently reported second generation HER2 affibody, $Z_{HER2:41071}$, replaced the –NDA– with an –SES– sequence at the C-terminal. Single photon emission computed tomography (SPECT) imaging of the [^{99m}Tc]Tc-$Z_{HER2:41071}$ tracer showed a significantly lower renal uptake by 25–30 fold (5.9 ± 2.1% ID g^{-1}), as well as a tumor-to-blood ratio of 363 ± 84 in SKOV-3 xenografts in contrast to [^{99m}Tc]Tc-ZHER$_{2:2395}$ (renal uptake and tumor to blood ratios are 183.8 ± 27.3% ID g^{-1} and 121 ± 24, respectively).[36] Given the precise quantification for HER2 expression and no obvious systemic side effects, it was favorable to adjust therapeutic schemes and monitor tumor progress.[37–39] More recently, a positron emission tomography (PET) imaging study performed in patients with advanced gastric cancer with low dose ^{68}Ga-NOTA-MALM-$Z_{HER2:342}$ showed a 3-fold higher lesion uptake compared with the HER2-negative group (SUVmax 10.5 ± 12.5 *vs.* 3.5 ± 1.7, $p = 0.005$) 2 h post-injection, without interference from simultaneous HER2 therapy.[40] Another bivalent affibody, ABY-027, was generated by fusing ABY-025 with an albumin-binding domain to improve the retention time and kinetic profile. Nevertheless, tumor tolerance to the HER2 targeted treatments may occur as a result of upregulation of HER3 (human epidermal growth factor receptor 3) receptors. ^{89}Zr-DFO-$Z_{HER3:8698}$ has been used to track the expression of HER3 after heat shock protein 90 kDa (Hsp90) inhibitor-AUY922 treatment.

‡ Fig. 2 is reproduced from ref. 35, annotation for HER2 positive or negative and different tracers used in each group has been added to the top and bottom of the cited figure (CC BY-NC link (**https://creativecommons.org/licenses/by-nc/4.0/**)); Fig. 3 is reproduced from ref. 75, the missing background part of the bottom right corner was filled without any information interference to the original picture (CC BY link (**https://creativecommons.org/licenses/by/4.0/**)); Fig. 4 is reproduced from ref. 100 (CC BY link (**http://creativecommons.org/licenses/by/4.0/**)); Fig. 5 is reproduced from ref. 123 (CC BY link (**http://creativecommons.org/licenses/by/4.0/**)); and Fig. 6 is reproduced from ref. 147 (CC BY link (**http://creativecommons.org/licenses/by/4.0/**)).

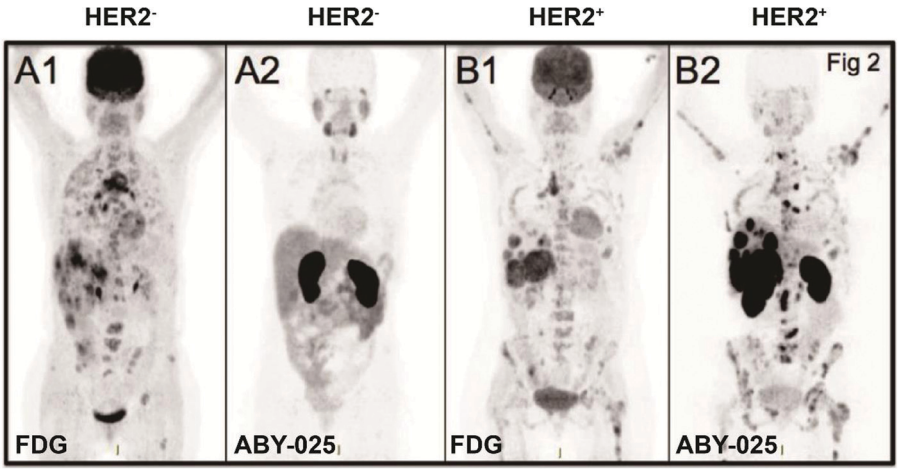

Fig. 2 HER2-specific-affibody imaging in the clinical trial. Notes: PET imaging of HER2-negative patients (A) and HER2-positive patient (B) with ^{18}F-FDG (A1, B1) and ^{68}Ga-ABY-025 (A2, B2); standard uptake value (SUV) is normalized to 10 for all images; darker colors indicate higher uptake. Specific uptake and high contrast image is shown with ^{68}Ga-ABY-025 compared to ^{18}F-FDG-PET image. Adapted from ref. 35. Abbreviations: HER2, human epidermal growth factor receptor 2; ABY, affibody; SUV, standard uptake value; PET, positron emission tomography; and FDG, fluorodeoxyglucose.

The results demonstrated favorable HER3 quantification by PET imaging, making it possible to evaluate and predict HER2-targeted therapy efficacy.[41] Moreover, the optimized HER3-specific probe [^{57}Co] Co-(HE)3-Z_{HER3}-DOTA significantly improved imaging contrast and prolonged tumor retention for up to 24 h in BxPC-3 xenografts *via* SPECT imaging.[42] Another epidermal growth factor receptor (EGFR)-binding affibody ABY-029 ($Z_{03115\text{-}Cys}$), labeled with an NIR (near-infrared ray) dye (IRDye® 800CW), provided an excellent *in vivo* imaging effect for glioma in nude mice. Meanwhile, early phase I studies of ABY-029 for gliomas, sarcomas, and head and neck cancers had completed (NCT02901925, NCT03282461, NCT03154411).[43–46] Detecting the insulin-like growth factor 1 receptor (IGF-1R) expression level is essential for assessing therapeutic efficacy and prognosis. To overcome the non-specific accumulation of the first anti-IGF-1R affibody imaging probe ^{111}In-DOTA-$Z_{IGF1R:4551}$, a novel IGF-1R-specific affibody $Z_{IGF\text{-}1R:4:40}$ labeled ^{64}Cu was used. The results showed significantly reduced non-specificity, low background imaging interference, and the majority being excreted from the kidneys and urinary systems in a glioma mice model.[47] Volunteers were recruited for tumor PET imaging with ^{68}Ga-NODAGA-$Z_{IGF\text{-}1R:4:40}$ (NCT02916394). The radiolabeled tracer 18F-NOTA-$Z_{PD\text{-}L1\_1}$ specific for programmed death-ligand 1 (PD-L1) exhibited high specificity to PD-L1, quick clearance, and good imaging contrast for mixed tumor-bearing mice *via* PET imaging, which is consistent with the results of immunohistochemistry; therefore, this tracer may have potential for use in clinical PD-L1 detection.[48] Recently, $Z_{CAIX:2}$ and $Z_{CAIX:4}$ affibody molecules were screened against a prognostic tumor marker, carbonic anhydrase IX (CAIX). The radionuclide imaging probes ^{99m}Tc-(HE)3-$Z_{CAIX:2}$ and ^{125}I-$Z_{CAIX:4}$ were evaluated in a mouse model, and demonstrated a high tumor tissue intake and a favorable tumor–blood ratio for clearly delineating the tumor.[49] Additionally, the biomarker B7-H3 (CD276), which is highly expressed in breast cancer, was combined with indocyanine green (ICG) and microbubbles (MB) to generate $ABY_{B7\text{-}H3}$-ICG and $MB_{ABY\text{-}B7\text{-}H3}$ for photoacoustic imaging, which demonstrated enhanced contrast signal and deep imaging effects in a mammary tumor model.[50,51]

Although no affibodies have been tested for cancer therapy in the clinic alone, many ongoing preclinical cancer studies for drug delivery or theranostics combined with affibodies have achieved promising results. For instance, the $(Z_{HER2:2891})_2$-ABD-MC-DM1 conjugates efficiently delivered the cytotoxic maytansine to HER2 over-expressed tumor tissue and demonstrated high uptake rates and potent ablation efficacy, which prolonged the survival time of mice.[52] A triple-modal (MRI/MSOT/CT) theranostic platform was built with Au–Fe_2C Janus nanoparticles and $Z_{HER2:342}$, which achieved deeper penetration and selective accumulation in mice tumor tissues, thus conferring high contrast imaging and efficient tumor ablation *via* photothermal therapy.[53] Furthermore, NIR-830-$Z_{HER2:342}$-IONP-Cisplatin theranostic nanoparticles exhibited substantial inhibition of primary and peritoneal metastatic tumors in an ovarian cancer mouse model, highlighting their potential to solve the defects of traditional debulking surgery.[54] TAM-HER3, a bivalent HER3-specific affibody, drastically suppressed heregulin-induced phosphorylation, effectively blocked receptors in HER3-positive tumor, and presented equal therapeutic efficacy and safety compared to seribantumab.[55] Besides, to overcome off-target effects triggered by nanoparticle cytotoxicity, a bioactivatable GSH-responsive nanogel decorated with anti-EGFR affibody was shown to specifically accumulate and internalize in the tumor tissue, ultimately realizing controllable photosensitizer release under a low GSH concentration intratumor environment for photodynamic therapy.[56] Liposome-coated doxorubicin coupled with $Z_{EGFR:1907}$ also provided a safe drug delivery platform with low cytotoxicity and improved antitumor efficacy.[57] Moreover, $Z_{PDGFR\beta}$ affibody was fused to the N-terminus

of mouse TNFα and conjugated with doxorubicin; it efficiently permeated the pericytes of PDGFRβ (platelet-derived growth factor receptor β) positive tumors and accumulated in the tumor lesion. This method of drug delivery showed desirable antitumor efficacy and tumor vessel reshape, potentially due to the reduced secretion of VEGF and increased level of intercellular cell adhesion molecule-1.[58] The $Z_{PDGFR\beta}$-IR700 probe has also been used for photodynamic therapy for colorectal cancer.[59] $Z_{HPV16E7}$ is the recently discovered affibody specific to HPV16 positive tumors; combined with exotoxin A, $Z_{HPV16E7}$ affitoxin384 exhibited significant tumor ablation in a cervical cancer mice model.[60] More recently, an affibody against the latent membrane protein 2 (LMP-2) associated with Epstein-Barr virus-induced tumors was fused with exotoxin for toxin delivery. $Z_{EBVLMP\text{-}2142}$–Z142X affitoxin showed potent cytotoxicity and favorable antitumor efficacy in LMP-2-expressed xenograft mice.[61]

ANTICALIN®

ANTICALIN® scaffolds are a class of affinity molecules engineered from small extracellular proteins, lipocalins, which recognize small hydrophobic molecules and cell surface receptors for transportation, mediating the immune response, or allergens and hormones.[62] Cup-shaped lipocalins consist of eight antiparallel β-strands, forming a β-barrel rigid framework, a single α-helix linked to the c-terminal, and four variable loops exposed on the surface, which constitute the binding pocket. The sequence and length diversity of loops provide the possibility for engineering new affinity ligands, the so-called anticalins.[63] The first reported ANTICALIN® was based on the butterfly-derived bilin-binding protein (BBP), which was reshaped to combine fluorescein.[64] To improve the safety and decrease the immunogenicity for human disease study, tear lipocalin (Tcl/Lcn1) and the neutrophil-gelatinase associated lipocalin (NGAL/Lcn2), with high compatibility and flexibility, were applied to construct human ANTICALIN® libraries.[65] The "Pieris" company, which has nine ongoing ANTICALIN® projects, has committed to realizing their commercialization since 2001, and many anticalins have also been reported in preclinical research.[66–68] However, only a few anticalins that are specific to biomarkers, including MET, HSP70, VEGF-A, VEGFR-3, PSMA, CD137, CD98, and ED-B, have been investigated for detecting or treating cancer.

An early study of PET tracer ^{89}Zr-PRS-110 for MET (hepatocyte growth factor receptor) imaging showed specific and low background imaging effects in the MET-expressing tumor models, which demonstrated the feasibility of ANTICALIN® as a targeting moiety for *in vivo* diagnosis.[69] Anticalins (N7A, N7E, and N9B) against fibronectin ED-B (extra domain B), which is uniquely expressed in neogenic blood vessels, labeled with a γ-emitter ^{123}I, presented high specificity and affinity to over-vascularized glioblastoma multiforme, as verified by histochemistry and *in vitro* autoradiography.[70] Later, a ketone group was introduced into ANTICALIN® N7A for conjugation with Alexa 488, which realized safe ED-B detection at the cellular level and demonstrated its potential as an *in vivo* imaging probe.[71] Meanwhile, prostate-specific membrane antigen (PSMA) and vascular endothelial growth factor receptor-3 (VEGFR-3)-specific anticalins combined with immunofluorescence staining were shown to exhibit high binding affinity and selectivity to PSMA- and VEGFR-3-positive cells, demonstrating the potential of these anticalins for further *in vivo* imaging and therapy studies of solid tumor.[72,73] The 70 kDa heat-shocking protein (HSP70) is commonly expressed in primary and metastatic tumors and is commonly upregulated after radiochemotherapy treatment. HSP70 PET imaging with the ^{89}Zr-labeled HSP70-binding ANTICALIN® BBG10C/I revealed deep tissue penetration and selective enrichment in mouse tumor sites. Moreover, strong *in vitro* tumor inhibition was realized by conjugating BBG10C/I with the toxin gelonin.[74] The latest published ANTICALIN® P3D11, which targets a malignant tumor marker, human CD98hc ectodomain (hCD98hcED), was examined in the first CD98 *in vivo* imaging study by labeling with ^{89}Zr and PASylation modification. The PET imaging performance was investigated in a prostate carcinoma xenograft-bearing mouse model and showed picomolar affinity, high tumor lesion accumulation (8.6 ± 1.1% ID g^{-1}), and a good tumor-to-blood ratio of 11.8 (Fig. 3).[75,76]

The most widely studied ANTICALIN® for cancer treatment is PRS-343 against a crucial costimulatory immune receptor 4-1BB/CD137, which plays a critical role in mediating the immune response and is typically expressed on tumor-infiltrating lymphocytes.[77] To safely activate T cells and reduce damage to the peripheral tissue of the tumor, the anti-HER2 monoclonal antibody trastuzumab was fused to the 4-1BB-specific ANTICALIN®; this dual-targeting fusion protein selectively accumulated in the tumor tissues and site-specifically activated tumor-localized T cells to achieve excellent tumor regression efficacy in a SKOV3 mouse model. The peripheral toxicity and pharmacological profile

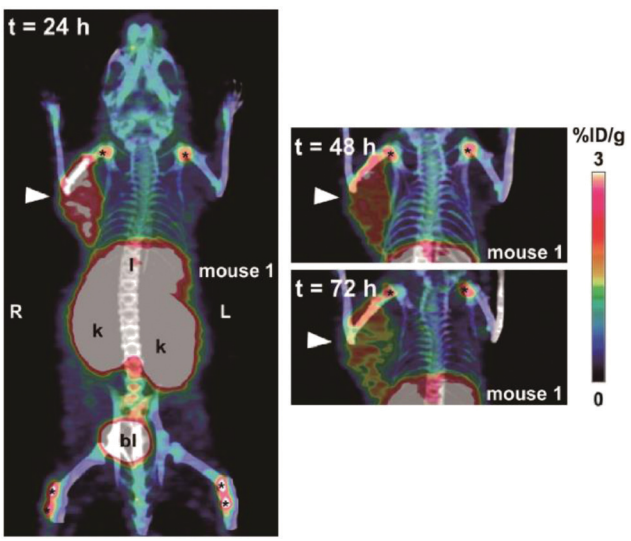

Fig. 3 *In vivo* PET study of CD98hc-binding ANTICALIN® tracer. Notes: prostate cancer xenografts mice were injected intravenously with ANTICALIN® probes D11vs-PAS200-Dfo ^{89}Zr; PET imaging data are acquired at 24 h, 48 h, and 72 h post-injection. Strong imaging signal is shown at 24 h (arrowhead) and gradually reduced at 48 h and 72 h; * indicated joints. Adapted from ref. 75. Abbreviation: l, liver; k, kidneys; and bl, bladder.

of PRS-343 have been verified in cynomolgus monkeys and in a mouse toxicology model.[78] A phase I trial of PRS-343 for patients with advanced HER2-positive tumors has been completed, and phase II studies of the combination with tucatinib, ramucirumab, and paclitaxel are currently recruiting (NCT03330561, NCT05190445).[79–82] Meanwhile, PRS-342 consisting of α-Glypican 3 antibodies fused to 4-1BB-specific ANTICALIN® also showed strong suppression of tumor growth and activation of T cells in a hepatocellular carcinoma mouse model.[83] Moreover, the 4-1BB-specific ANTICALIN® combined with PD-L1 inhibitor (atezolizumab) achieved excellent co-stimulation efficacy for immune system activation in the tumor microenvironment and successfully ablated tumor cells in a mouse model. A phase II trial (NCT05159388) for combination therapy of this fusion protein (also called PRS-344) is currently recruiting. Additionally, the phase I study (NCT01141257) of ANTICALIN® PRS-050-PEG40 (Angiocal) against VEGF-A was completed in 2013. Clinical data have shown safety and efficient inhibition of angiogenesis by reducing MMP-2 in patients with advanced solid tumors.[84] Later, PEGylated PRS-050 was evaluated in A673 sarcoma xenografts, and was shown to strongly block vascular permeability and reduce microvessel density to inhibit tumor growth. This compound provided favorable safety with no side effects of platelet aggregation and thrombosis resulting from bevacizumab therapy.[85]

Adnectin/monobody

Fibronectins are a type of macro-glycoprotein that widely exist in animals and are responsible for intercellular communication and constitute the extracellular matrix. One of the major components of human fibronectins is the tenth fibronectin type 3 domain (^{10}FN3), a subfamily of immunoglobulin superfamily composed of seven β-strands, which forms a β-sandwich framework connected by six loops, three of which are variable.[86] As their structural features resemble those of the variable heavy chains of antibodies, ^{10}FN3 was engineered as a novel protein binder, termed monobody (10 kDa).[87] The first devised ^{10}FN3 scaffold against ubiquitin was generated by mutating residues in the BC and FG loops, while the DE loop was introduced later for screening the TNF-α binding ligand.[88] The commercialized monobody was named Trinectin by the ''Adnexus'' company, which was then acquired by ''Bristol-Myers Squibb'' and renamed Adnectin in 2007.[89] A conventional loop-based adnectin library was designed by randomizing residues within the BC, DE, and FG loops of ^{10}FN3. Later, side-and-loop-based libraries were constructed by reshaping the second CD-FG β-sheets, which formed a concave binding pocket suitable for convex receptor epitopes, such as globular macromolecules.[90] Currently, more than 50 adnectin molecules have been selected and used in biological or medical research.[91,92]

Anti-vascular endothelial growth factor receptor 2 (VEGFR2) adnectin CT-322/BMS-844203/FN3$_{VEGFR2}$ is the first one to enter the clinic trial, showing a good pharmacokinetic profile and safety (NCT00374179).[93] Functionalizing with molecularly targeted MB generated an ultrasound imaging probe, MB-FN3$_{VEGFR2}$, which showed high affinity, selective accumulation, and strong ultrasound signal in a breast cancer mouse model.[94] Another adnectin E1 against human EphA2, which is aberrantly expressed in diverse cancers, was used in an *in vivo* imaging study of the fluorescent probe E1-Rluc8 and a radiolabeled tracer ^{64}Cu-NOTA-E1 in a subcutaneous prostate tumor model, with results showing a strong signal, selective accumulation, and rapid clearance.[95,96] So far, two anti-PD-L1 adnectins, FN3hPD-L1-01 and BMS-986192, have been investigated for PD-L1 imaging, and the latter has shown good results in the clinic. ^{64}Cu-FN3hPD-L1 exhibited high specificity and a tumor-to-muscle ratio of 13 after 4 h in mice for PD-L1 expression quantification.[97,98] Moreover, the PET imaging probe ^{18}F-BMS-986192 showed picomolar binding affinity, spleen accumulation, and rapid clearance from the kidneys and bladder in healthy cynomolgus monkey, and favorable dosimetry results provided an estimated safe dose for human use of 2.20×10^{-1} mSv/MBq. The *in vivo* study of ^{18}F-BMS-986192 in HT-29 and L2987 xenograft models presented peak radioactivity of tumor tissue 25 min post-injection and low background imaging for PD-L1 expression evaluation.[99] Human study of PD-L1 whole body quantification for patients with terminal non-small cell lung cancer (NSCLC) was completed with ^{18}F-BMS-986192, which exhibited safe pharmacokinetic performance and accurately detected the heterogeneity of PD-L1 distribution between individuals and diverse tumor lesions compared to the results of conventional biopsies. A phase I study on ^{18}F-BMS-986192 PET imaging in patients with oral cavity squamous cell carcinoma is ongoing (NCT03843515) (Fig. 4).[100,101] A PD-L1 PET imaging pilot study (NCT03520634) also demonstrated that ^{18}F-BMS-986192 provided a baseline uptake for predicting the lesion volume recession effect after immune checkpoint inhibitor treatments.[102]

In terms of cancer therapy, a phase I trial of CT-322 demonstrated significant blocking of VEGFR2 receptors and

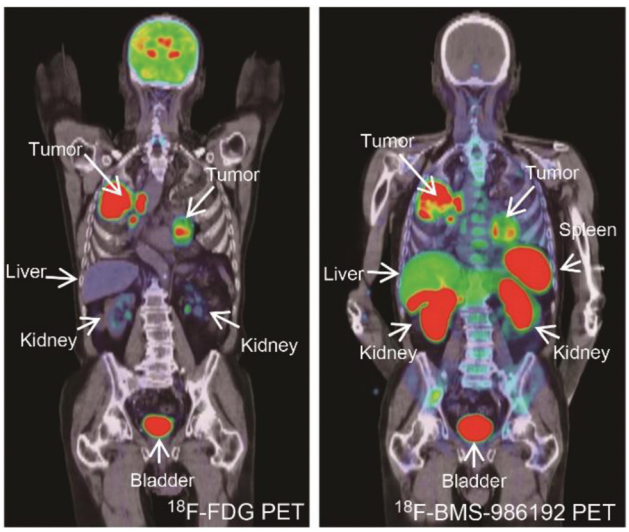

Fig. 4 PD-L1-targeting adnectin probes for clinical PET imaging. Notes: a patient with advanced NSCLC (PD-L1 expression >50%) was administered with ^{18}F-FDG PET (left) and ^{18}F-BMS-986192 adnectin PET tracer (right); compared to the FDG tracer, the PET image of adnectin showed high tumor-to-background contrast and heterogeneous uptake at tumor sites. Adapted from ref. 100. Abbreviations: NSCLC, non-small-cell lung carcinoma; and PD-L1, programmed death-ligand 1.

efficient inhibition of angiogenesis and metastasis in solid tumors, although it failed to treat recurrent glioblastoma in a phase II study.[103] Later, CT-322 modified by PASylation demonstrated a significant boost in bioactivity, pharmacokinetic properties, and half-life extension in a mouse model than PEGylation, thus providing a safe and effective drug delivery system for further clinical study.[104] EGFR-specific adnectin-E3 has also been used to engineer a new chimeric antigen receptor T cell system; this adnectin-based CAR-T, which showed lower immunogenicity and improved selectivity and safety, offered equivalent tumor ablation efficacy in an immunodeficient NSG mouse model in contrast with the conventional scFv-based CAR system.[105] Another adnectin, Mb(S4), against WDR5 (necessary for the mixed-lineage leukemia 1 [MLL1] methylation), was genetically encoded with a TMP-inducible expression system as an inhibitor for WDR5–MLL1 interaction, and functioned to reduce methyltransferase activity, downregulate MLL1 relative gene expression, and extend survival in the MLL-AF9 leukemia model.[106] The RAS binding adnectin NS1 could intervene in the α4–α5 subunit interface to inhibit RAS activation, and combined with a doxycycline-inducible expression system, presented a good antitumor effect in a mouse model.[107] Glypican-3-specific adnectin A1 conjugated with the microtube inhibitor tubulysin showed effective tumor regression in Hep3B xenografts, which persisted for 2 weeks.[108] More recently, a mesothelin-binding adnectin was reported with the ability to induce apoptosis and, combined with mitomycin C, showed a strong tumor inhibition efficacy in A431 cells.[109]

Designed ankyrin repeat proteins (DARPins)

Ankyrin repeat (AR) proteins with helix–loop–helix conformations are present in virtually all phyla and are exclusively involved in mediating protein–protein interactions, including transcription, ion transportation, and cell cycle modulation.[110] Crystal structure and consensus sequence analyses of the ankyrin motif revealed that the conserved hydrophobic core of the α-helix constituted rigid elements, while the less conserved loop region of solvent-accessible surface contributed to molecular recognition, which forms the basis of the protein binder design.[111] DARPin scaffolds comprise 2–3 human AR motifs flanked by capping repeats at both the N- and C-terminals, which protect them from aggregation during the folding process. Each AR unit (33 amino acids) is composed of two antiparallel α-helices with a loop and a β-turn extended from each end for binding to the next AR, and 6–7 residues within each repeat are available for randomization.[112] Based on the consensus design strategy, a biopharmaceutical company called "Molecular Partners AG" founded in 2004 has developed new DARPin molecules as antibody alternatives for clinical translation.[113] Moreover, a loop-DARPin library was constructed by introducing the CDR-H3 domain of antibodies to solve the limitations of traditional DARPins, including the less convex and somewhat rigid binding surface.[114] Until now, more than 60 DARPin molecules have been reported, and owing to their small size (14–18 kDa), physicochemical stability, and ease for producing multivalent or multispecific targeting elements, DARPins have become attractive for diagnostic and therapeutic applications.[115,116]

The Cy5.5-labeled DARPin 8h6 was the first reported DARPin-based fluorescent probe for *in vivo* imaging study. This probe is specific for cathepsin B, which is overexpressed in the tumor microenvironment, and shows a strong long-term signal ratio up to 72 h in a breast cancer model, despite partial liver accumulation.[117] Moreover, HER2-specific DARPins G3, 9_29 labeled with fluorescein and a radionuclide, respectively, exhibited a good tumor-tissue ratio and high contrast SPECT imaging effect in a HER2-positive malignant tumor model. Moreover, the superparamagnetic nanoparticle probe SPIO-G3-5MF and upconversion nanoparticle UCNP-PMAO-DARPin-9_29 were effective in diagnosing SKBR-3 xenograft tumor models, with selective accumulation and long-term retention.[118,119] Furthermore, DARPin G3 was genetically displayed on the surface of exosomes and radiolabeled with ^{99m}Tc to take advantage of the DARPin specificity and the homing ability of exosomes. Planar imaging has shown that these probes rapidly accumulated in breast cancer, with a high contrast signal detected for visualizing tumor lesions.[120] The phase I SPECT imaging study in patients with primary breast cancer (NCT04277338) proved that the ^{99}mTc-$(HE)_3$-G3 tracer had good tolerability, biodistribution, and ability to discern HER2 positive or negative tumor.[121] Moreover, the newly reported imaging probe ^{125}I-PIB-H6-Ec1 selectively binds to the biomarker EpCAM (epithelial cell adhesion molecules) with picomolar affinity based on the DARPin molecule Ec1. In an *in vivo* xenograft mouse model, this probe demonstrated lower non-specific accumulation and favorable tumor-to-organ ratios for tumor imaging (Fig. 5).[122,123]

MP0250 DARPin against HGF, VEGF-A, and human serum albumin is the first tri-specific DARPin. A clinical phase II program (NCT02194426) demonstrated the good tolerability

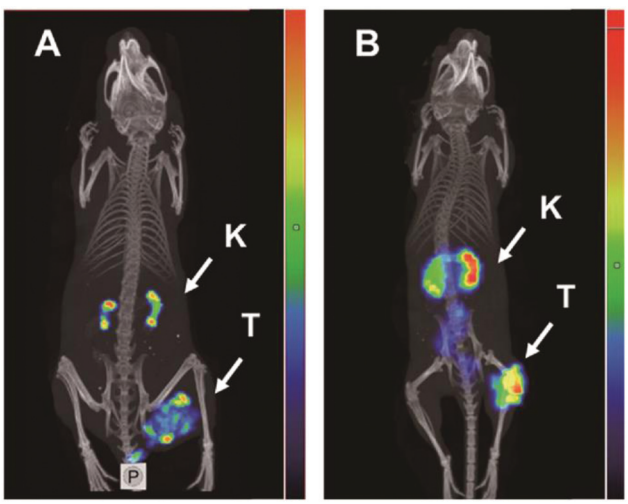

Fig. 5 *In vivo* SPECT imaging of EpCAM-specific DARPins probes. Notes: OVCAR-3 (A) and SKOV-3(B) xenografts models; mice are injected with the DARPin probe [^{125}I] I-PIB-Ec1 and imaged at 6 hours post-injection. High contrast tumor imaging and mainly cleared through the kidneys has shown. Adapted from ref. 123. Abbreviations: SPECT, Single-photon emission computed tomography; EpCAM, epithelial cell adhesion molecules; DARPins, designed ankyrin repeat proteins; K, kidneys; and T, tumors.

and pharmacokinetic properties of MP0250 in patients with advanced solid tumors, in which 14 patients showed slight tumor shrinkage.[124–126] Moreover, MP0250 has completed another phase II trial for patients with multiple myeloma with the combinational therapy of bortezomib and dexamethasone (NCT03136653).[127,128]

More recently, a MET antagonist of DARPins was shown to tightly bind two epitopes of the extracellular domain of MET and efficiently block MET-dependent signaling pathway activation and inhibit proliferation in gastric carcinoma cells.[129] Moreover, the EGFR-specific DARPin-E01 fused with the TPD prodomain avoided EGFR–ligand shedding by inhibiting A-disintegrin and metalloproteinase. The fusion protein E01-GS-TPD potently blocked EGFR receptors and reduced their kinase activity, showing significant inhibition of tumor cell proliferation and migration *in vitro*.[130] Another study genetically modified oncolytic measles virus with EGFR-binding DARPins E.01 and MMPA1 activated by tumor-associated MMPs. The bi-specific engineered virus MV-MMPA1-E.01 displayed reduced off-target effects and demonstrated favorable therapeutic efficacy in GBM xenograft models.[131] HER2-specific DARPins have also been broadly studied for cancer treatment. For instance, the hybrid upconversion nanoparticles, UCNP-R-T, composed of radionuclide ^{90}Y and exotoxin A, and anti-HER2 DARPin-PE40 generated nanotheranostic regents achieved background-free imaging and effective tumor ablation in a breast cancer mouse model.[132] Patients with HER2-positive solid tumors were recruited for a phase I study with the HER2-binding DARPin drug MP0274 (NCT03084926).

EpCAM, EGFR, and HER2-targeting DARPins used to engineer monospecific and multispecific CAR-T cells showed desirable antitumor efficacy equivalent to scFv-based CAR-T cells, and the multispecific CAT-T cells reduced antigen escape and enhanced synergistic effect of immunotherapy in different NSG mouse xenograft models.[133,134] The DARPin molecules TREG005 and TREG006 serve as agonists to TNFR2 (CD120b) of tumor-infiltrating T cells, and have been shown to strongly activate the NF-κB signaling pathway *in vitro*, and facilitate $CD8^+$ T cell infiltration into tumor tissue and enhance IFN-γ expression in an *in vivo* model.[135] MP0310 (AMG506) and MP0317 are bispecific DARPin scaffolds against 4-IBB (CD137) and CD40, respectively, and have been combined with the fibroblast activation protein to activate the tumor-localized immune response in an actively recruiting phase I study (NCT04049903, NCT05098405).

Knottin

Knottin molecules are a subclass of the cystine-knot miniprotein family, which broadly exists in many plants, animals, and fungi in the form of inhibitors that play essential roles in mediating signaling transduction, channel blocking, and proteolysis inhibition.[136,137] The knottin scaffold consists of three antiparallel β-strands and three disulfide bonds (I–IV, II–V, and III–VI) with several exposed variable loops; generally, the third disulfide bond threads through a macrocycle, which was constituted by the first two disulfide bonds and then formed a constrained knot structure. This rigid knot fold confers its excellent structural stability to temperature, proteolysis, and chemical denaturation; besides, good sequence tolerance has been shown given that the sequence identity of the knottin motif is very low, excluding the six cysteines.[138] It is worth noting that the knottin molecule can be produced in microbes, despite the existence of disulfide bonds. Aside from the above advantages, small size knottin scaffolds (<4 kDa) also show good pharmacological properties, targeting specificity and non-immunogenicity. Knottin scaffolds were engineered as new protein binders for devising targeting imaging probes and drug delivery systems.[139,140] Knottin scaffolds are being explored by several companies, including ''Jazz,'' ''Ironwood,'' ''Cyclogenix,'' and ''AstraZeneca,'' and some FDA-approved knottin-drugs like ''Ziconotide'' and ''Linaclotide'' have been marketed although not for cancer.[141–144] Currently, most reported knottin scaffolds originate from animals and plants, and a few have been used to construct knottin display libraries. While grafting with known binding motifs as agonists or antagonists is more prevalent, partial mainstream knottin scaffolds have also been reported.

The most commonly investigated knottin scaffold for tumor imaging and therapy is integrin-targeting integrin αvβ6 binding knottin (R01-MG) labeled with the contrast agent A740. This scaffold has been used for photoacoustic and fluorescence imaging in A431 xenograft mice, in which maximal signal and significant contrast enhancement were observed in tumor tissues after 1 h, demonstrating rapid localization and good imaging effect.[145] R01-MG-IRDye800 has also been evaluated in subcutaneous and orthotopic tumor models, with results showing a higher tumor-to-background ratio of 2.5–2.7. Furthermore, a strong contrast fluorescent signal under 750 nm laser exposure for 30 min proved its ability for imaging-guidance surgery and potential for further clinical application.[146] More recently, three PET tracers based on R01-MG, [^{18}F]FDG and [^{18}F]FP-R01-MG-F2, and [^{68}Ga]NODAGA-R01-MG have been evaluated in patients with pancreatic, lung, or cervical cancer and healthy volunteers, which demonstrated their safety, selective and quick accumulation in tumor tissues, and low background interference imaging for cancer diagnosis (NCT02683824) (Fig. 6).[147] Another knottin scaffold (MC-FN-010) against the extra domain B of human fibronectin, which is associated with tumor angiogenesis, conjugated to Alexa Fluor 680, presented a significant uptake and favorable imaging capacity in glioblastoma mouse models.[148]

EETI-2.5F knottin against integrin receptors (αvβ3, αvβ5, and α5β1) was dimerized through oxime-conjugation, the dimer 2.5_AO reached a 150-fold binding affinity improvement compared to the monomer and more effectively inhibited glioblastoma and breast cancer cell proliferation and migration *in vitro* compared to clinical cilengitide.[149] EETI-2.5F modification helps the cell cycle inhibitor gemcitabine to evade its resistance in pancreatic cancer cells, and the drug conjugate was efficiently released intracellularly, which achieved potent suppression of tumor growth *in vitro* and demonstrated its potential for targeted drug delivery.[150] EETI-2.5F combining with the tubulin inhibitor MMAF, EETI-2.5F-Fc-MMAF, efficiently suppressed tumors and extended the mice's survival time in the

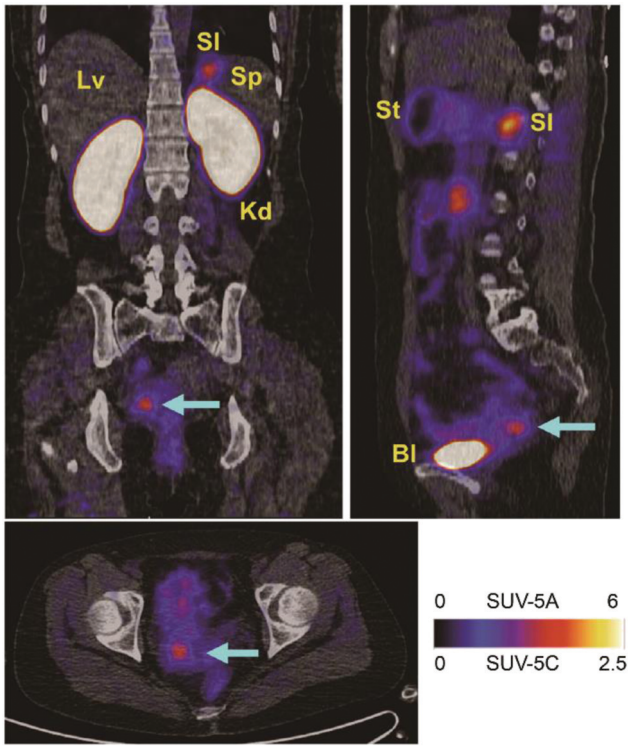

Fig. 6 αvβ6-Targeting Knottin tracer of PET/CT imaging in the clinical trial. Notes: a cervical cancer patient was administered with Knottin probe 68Ga-NODAGA-R01-MG; cervical tumor pointed by the cyan arrowhead and SUV_{mean} reached 4.79 ± 0.37. Adapted from ref. 147. Abbreviations: Lv, liver; Sp, spleen; Bl, bladder; Kd, kidneys; Si, small intestine; and St, stomach.

U-87 MG xenograft model when administered at 10 mg kg^{-1} twice a month.[151] Furthermore, the oncolytic measles virus (MV) modified with EETI-2.5F was intravenously injected into a glioblastoma mouse model and showed excellent antitumor efficacy.[152] Additionally, another natural knottin molecule, chlorotoxin/CTX, isolated from scorpion venom, can permeate through the blood–brain barrier easily and specifically accumulate in neuroectodermal tumors.[153] Ribosome inhibitor gelonin fused with chlorotoxin significantly suppressed the translation process in U-87 MG cells, with lower toxicity and strongly ablated tumor tissue performance in the U-87 MG xenograft mice.[154] The PET tracer ^{18}F-FP-chlorotoxin is rapidly taken up by the MMP-2 expressed glioma at 90 min post-injection and showed a high contrast imaging effect.[155] Chlorotoxin-ICG, also called BLZ-100/tozuleristide, was tested in spontaneous canine tumors, and exhibited a 20-fold tumor-to-tissue contrast for intraoperative imaging.[156] Medulloblastoma imaging with BLZ-100 enhanced signal contrast between the tumor core and margins for clear tumor delineation.[157] A phase I trial of BLZ-100 for recurrent gliomas has shown safe dose tolerability up to 30 mg in humans, while further phase II/III trials are ongoing (NCT02234297, NCT03579602).[158]

Other scaffolds

In addition to the scaffolds described above, some other less developed or emerging scaffolds have been reported for cancer research.

Kunitz

The kunitz scaffold (~7 kDa) was engineered from protease inhibitors with a rigid α-helix and β-sheet folds that are structurally constrained by three disulfide bonds.[15] The "Shire (Dyax)" company has explored kunitz molecules for commercialization.[159] A few Kunitz-type scaffolds, angiopep-2 (ANG) for glioblastoma imaging, Amblyomin-X for tumor inhibition *via* regulating Rho-GTPases and uPAR signaling, and APPI-4M blocking the invasion of KLK6-dependent breast cancer *in vitro*, were reported.[160–162]

Affimer. Another scaffold, affimer (~14 kDa), derives from the human stefin A protease inhibitors with an α-helix over four antiparallel β-sheets and two-variable loops.[163] Affimer scaffolds are currently being developed by "Avacta Life Sciences".[164] Recently, HER4 binding affimer 5 conjugated with CF640R-maleimide fluorescent dyes have been tested for imaging of MCF7 cells *in vitro*. The VEGFR2-specific affimer B8 and A9 were labelled with biotin as probes and presented higher sensitivity in histochemical staining assay compared to the commercial VEGFR2 antibody.[165,166]

Nanofitin. The nanofitin scaffold (7 kDa), also called affitin, originated from the DNA binding protein *Sac7d* family and was first commercialized by the "Affilogic" company.[167,168] Engineered EGFR-specific nanofitin B10 has been used to generate the radiolabeled probe ^{18}F-FBEM-Cys-B10, which provided excellent imaging results in the A431 tumor model.[169]

Avimer. An avimer scaffold based on the A-domain of diverse membrane receptors is another antibody memetic that has been explored by the "Amgen" company.[170,171] Recently, a previously reported C426 avimer scaffold has been designed as a novel C-MET reporter by introducing a gly_3-cys sequence at the c-terminal. Although the computational model and ELISA showed good traceability, further *in vivo* study is needed.[172]

Centyrins. Centyrins are derived from the Fn3 domains of the tenascin scaffold, and the "Janseen" company is currently exploring the commercialization of centryins.[173] The EGFR-specific centyrin 83_V2 conjugated with the tubulin inhibitor MMAF exhibited potent cytotoxicity in NCI-H1573 cells. Simultaneously, 83v2 labeled with the NIR dye S0456 localized at the tumor lesion after 4 h, and showed a long retention time beyond 24 h, with a high contrast imaging effect observed in xenograft mice.[174,175]

Affilin. Ubiquitin molecules (~76 amino acids) comprising an α/β secondary structure and molecular recognition function were engineered as affilin scaffolds and are currently being explored by the "Scil Proteins" company.[176,177] Moreover, HER2 and EGFR binding affilins fused to the anti-EGFR monoclonal antibody cetuximab have been shown to achieve bi-specificity and strong inhibition of cancer cell proliferation *in vitro*.[178]

ADAPT. The albumin-binding domain with good solubility generally extends the half-life of drugs or probes. Based on the interaction energy calculation, 11 variable residues on the surface were identified by alanine scanning, which were then engineered to albumin-binding domain-derived affinity protein (ADAPT).[179] An ADAPT6 scaffold specific to HER2 was labeled with a radionuclide and showed high contrast imaging *in vivo*

and better delineation for small metastases. Besides, ADAPT6 conjugated with exotoxin A (ETA) demonstrated excellent efficacy as a cancer therapeutic in a preclinical study.[180–182]

Design of protein scaffolds

Although protein scaffolds have acquired promising achievements in different application fields, it remains vital to devise or discover novel scaffold molecules considering the limitations of the protein scaffolds, such as patent monopoly, short half-life, immunogenicity, and less accessibility to the flat area of targets. One should keep in mind that a suitable candidate scaffold should possess a compact structure with a rigid core and good tolerance to residue substitution or engraftment without losing its structural integrity and stability.

Ligand mimicking is a mainstream design method, which requires engrafting known binding motifs onto scaffolds and reshaping scaffolds derived from a protein data bank (PDB) or *in silico.* Ligand mimicking consists of several parts: binding motif analysis, rational scaffold selection, computer simulation motif grafting, molecular docking, and further optimization of folding efficiency stability, and solubility.[183]

The motif sequence is based on the analysis of the ligand–receptor co-crystallization structure; normally, a consecutive sequence containing binding site is preferred. The flexible motifs are well accepted by most scaffolds; in contrast, one should consider whether the scaffold's conformational folding path matches with rigid motifs.[184] Searching scaffolds from the PDB databases or de novo design library, and comparing similarity *via* PDBeFold or DALI is a good option; meanwhile, small protein inhibitors also require attention, such as typical kunitz, affimer, and knottin scaffolds.[185] It should be noted that some *de novo* scaffolds may be difficult to be expressed in *E. coli* due to their evolutionary preference inconsistence.[186] Combining with molecular modeling (Rosetta) and thermodynamic simulation calculation, it is possible to produce rational motif–scaffold structures. Moreover, solubility and folding efficacy could be optimized by replacing soluble residues and employing the fold-from-loops strategy.[187,188] Candidate structures with high-affinity rates after multiple molecular docking comparisons are suitable for further expression and surface plasmon resonance (SPR) to verify their actual effects. Sometimes, low stability may affect correct folding, and it is worth trying to introduce disulfide-bridges with appropriate distances to improve the overall stability of the scaffolds.[184]

Tetsuya's group grafted two CD25-binding residues GGGV-D of daclizumab and YGY-RS-Y of basiliximab onto a zinc-finger peptide scaffold to construct a small antibody mimetic library, three CD25-binding ligands with 30 nM affinity were successfully selected.[189] Cassie's group designed PD-1 agonist by inserting three binding motifs ''WDYKY'', ''ADYKR'', ''WDYKR'' into 34840 de novo-designed scaffolds, after Rosetta, fold-from-loopsm, flow cytometry sorting and affinity maturation processed, an agonist PD-MP1 were selected, monomeric PD-MP1 showed 6 μM affinity to mouse PD-1, and trimeric PD-MP1 strongly inhibited murine T cell activation *in vitro*.[190] A helix-kinked-helix motif of PfEMP1 molecules which forms core binding site of endothelial protein C receptor was integrated to a three-helical bundle scaffold as a vaccine immunogen, the final binder could elicit antibodies, although not as effective as the whole CIDRalpha1 domain.[184]

Another approach scaffold reshaping is commonly involved in scaffold selection, solvent-accessible surface area calculation, stability evaluation, library construction, and binder panning verification.

First, existing scaffolds can be screened from the PDB by setting different criteria, such as the size range, human or microbe derived, cysteine-free or not, high-resolution, solubility (based on literature data), nontoxicity, and the number of loops, β-sheets or α-helices. The filtered results can be further refined by similarity alignments. Based on the FoldX platform, it is possible to calculate the energy difference of mutated surface residues to select diversified sites. Often loops with no specified structures tend to present a high solvent-accessible surface area that is suitable for randomization.[191] Next, stability assessment can be achieved *via* the Eris platform, disulfide-bridge, or other slat-bridge introductions, and should be considered in some cases.[192] Ideally, the diversified residues should be close in sequential and structural space, and libraries with good diversity require at least ten randomized sites in theory. Finally, it is possible to select designed scaffold binders against targets *via* experiments to evaluate their performance.[193,194]

Hackel's group searched ideal scaffolds from the PDB that conform to a series of criteria, 259 candidates were further evaluated *via* solvent accessible surface area calculation and destabilization after randomization; the T7 phage gene 2 protein (Gp2) with best rates was selected for library construction. Gp2 binder $GaEGFR_{2.2.3}$ (18 ± 8 nM) and $GP2\text{-}PDL1_{E4}$ (3–13 nM) against EGFR and PD-L1 were screened.[193,195] Schneider's group screened scaffold candidates from the PDB databases, after sequence alignment, in silico saturation mutagenesis, structural evaluation, the 4PSF scaffold was finally selected to build the ProBi library, ProBi binder against human interleukin-10 with nanomolar affinity was screened.[194]

To sum up, with the development of various technologies, such as computer-aided design, protein prediction (Alphafold, Rosetta), molecular docking, molecular dynamics simulation, crystallographic structural analysis, deep sequencing, and learning, designing novel protein scaffolds will be easier and more feasible.

Conclusions

Protein scaffolds as antibody alternatives have been widely investigated for cancer diagnosis and therapy in preclinical and clinical studies over the past two decades.

In comparison, some outstanding advantages of protein scaffolds are irreplaceable, except for the high affinity and specificity. For example, the smaller molecular size (<20 kDa) facilitates tissue infiltration and deeper tumor lesion penetration.[196] Protein scaffolds with small steric obstacles can easily access hidden epitopes located in the deep groove of some

undruggable targets, such as Ras and Myc, which is impossible to approach using conventional antibodies.[197–199] Moreover, the favorable physicochemical stability of scaffold binders is also appealing; generally, they can refold to their original structure after experiencing extreme temperature changes over 60 °C or following a broad range pH change (2.5–11). Some of them, such as knottin scaffolds, are able to withstand even higher temperatures (over 100 °C), making efficient coupling and photothermal reaction possible.[9] Besides, the knottin scaffolds also show fantastic stability after being exposed to protease from the gastrointestinal tract, which demonstrates their potential for oral administration.[200] No apparent affinity loss of protein scaffolds was found after modification with fluorescent dyes, radionuclides, and drugs compared to the antibody conjugates.[13] In addition, small scaffolds of <200 amino acids, library reshaping, site-directed mutation, and specific residue introduction are easier than antibodies *via* gene engineering. Meanwhile, considerable and homogeneous modified products can be well controlled by introducing cysteine residues or azide groups to provide a single coupling site.[201] Most importantly, protein scaffolds can be mass-produced *via* the prokaryotic expression system are more cost-effective and affordable for research and patients in the future.

Challenges

Despite some protein scaffolds showing promising performance in different fields, few can realize successful clinical translation for cancer imaging or therapy, partially due to their short half-life, immunogenicity, somewhat unspecific biodistribution, or other less good clinical effects during long-term different dose administration.

Small size scaffolds with a short half-life generally accelerate the extravasation rate, are rapidly cleared from the circulating blood system, and impair the tissue penetration efficacy. Therefore, strategies of retention time extension, such as PEGylation, PASylation, fusing with Fc fragments, or albumin-binding domain, should be considered.[202] Furthermore, immunogenicity resulting from non-human-derived scaffolds must also be resolved. Previous studies have demonstrated that constant region residue substitution (N23T, S33K, and N43E) of the HER2 affibody dramatically lowers the interaction with Ig and IgM, while some other residue replacements (D36A, D37S, E47A) have been shown to reduce the HER2 binding activity or thermostability.[203] Additionally, the randomized residue (Q32) of the affibody scaffold was directly involved in both the Fc and the V_H3 interaction; by systematically comparing the relationship between Q32 amino acid usage frequencies and the actual immunogenicity effect, it is possible to find the least immunogenic residues for this position. Biodistribution is another shortcoming; except in the metabolic organs, liver and kidneys, some scaffolds may cause unspecific accumulation, which results in a high imaging background or cytotoxicity, along with an increased residency time and dose. According to previous studies, hydrophilicity and charges seem to be the crux for biodistribution.[204,205] By replacing hydrophilic amino acids, the $Z_{HER2:34}$ affibody (A42S, A46S, A54S) showed significantly improved hydrophilicity, reduced renal retention by nearly threefold, and lowered the hepatic uptake. $Z_{HER2:V2}$ (N52S, D53E, A54S) also lowered the renal uptake by 25- to 30-fold compared to the original affibody.[36,206]

Prospects

Overall, protein scaffolds are promising alternatives with many favorable properties superior to antibodies. Besides, protein scaffolds have been widely applied not only in cancer imaging and therapy but also in basic research, such as detection and elimination of microbes, intracellular delivery, blocking of the signal pathway, crystallization analysis, and *in vitro* detecting probes. With the development of computer simulation, molecular docking, and experimental technologies, the inherent flaws of scaffold molecules are expected to be gradually reduced, and safer, more effective, and affordable novel scaffolds will emerge. We expect that protein scaffolds will provide us with more options for cancer diagnosis and therapy in the future.

Conflicts of interest

There are no conflicts to declare.

Acknowledgements

This work was partially supported by the Shanghai Municipal Science and Technology Major Project (ZC).

References

1 D. Senft, M. D. M. Leiserson, E. Ruppin and Z. A. Ronai, *Trends Mol. Med.*, 2017, **23**, 874–898.
2 E. R. Malone, M. Oliva, P. J. B. Sabatini, T. L. Stockley and L. L. Siu, *Genome Med.*, 2020, **12**, 8.
3 I. R. Konig, O. Fuchs, G. Hansen, E. von Mutius and M. V. Kopp, *Eur. Respir. J.*, 2017, **50**, 1700391.
4 M. Olivier, R. Asmis, G. A. Hawkins, T. D. Howard and L. A. Cox, *Int. J. Mol. Sci.*, 2019, **20**(19), 4781.
5 C. H. Chau, P. S. Steeg and W. D. Figg, *Lancet*, 2019, **394**, 793–804.
6 X. Zhao, Q. Ning, Z. Mo and S. Tang, *Artif. Cells Nanomed. Biotechnol.*, 2019, **47**, 3621–3630.
7 L. H. Butterfield, S. P. Schoenberger and J. B. Lyczak, *Immunology, Infection, and Immunity*, 2004, pp. 573–591, DOI: **10.1128/9781555816148.ch24**.
8 R. B. Corley, *Immunology, Infection, and Immunity*, 2004, pp. 111–143, DOI: **10.1128/9781555816148.ch6**.
9 X. Yu, Y. P. Yang, E. Dikici, S. K. Deo and S. Daunert, *Annu. Rev. Anal. Chem.*, 2017, **10**, 293–320.
10 Y. J. Lee and K. J. Jeong, *J. Biosci. Bioeng.*, 2015, **120**, 483–490.
11 M. C. Ochoa, L. Minute, I. Rodriguez, S. Garasa, E. Perez-Ruiz, S. Inoges, I. Melero and P. Berraondo, *Immunol. Cell Biol.*, 2017, **95**, 347–355.

12 Y. Wang, Z. Fan, L. Shao, X. Kong, X. Hou, D. Tian, Y. Sun, Y. Xiao and L. Yu, *Int. J. Nanomed.*, 2016, **11**, 3287–3303.
13 L. Eyer and K. Hruska, *Veterinarni Medicina*, 2018, **57**, 439–513.
14 A. Skerra, *J. Mol. Recognit.*, 2000, **13**, 167–187.
15 R. Simeon and Z. Chen, *Protein Cell*, 2018, **9**, 3–14.
16 D. Schumacher, J. Helma, A. F. L. Schneider, H. Leonhardt and C. P. R. Hackenberger, *Angew. Chem., Int. Ed.*, 2018, **57**, 2314–2333.
17 S. Massa, C. Xavier, S. Muyldermans and N. Devoogdt, *Exp. Opin. Drug Delivery*, 2016, **13**, 1149–1163.
18 S. Dickgiesser, R. Kellner, H. Kolmar and N. Rasche, *Methods Mol. Biol.*, 2019, **2033**, 1–14.
19 M. Morais, N. Forte, V. Chudasama and J. R. Baker, *Methods Mol. Biol.*, 2019, **2033**, 15–24.
20 G. Chaubet, F. Thoreau and A. Wagner, *Drug Discovery Today Technol.*, 2018, **30**, 21–26.
21 E. M. Milczek, *Chem. Rev.*, 2018, **118**, 119–141.
22 P. Adumeau, S. K. Sharma, C. Brent and B. M. Zeglis, *Mol. Imaging Biol.*, 2016, **18**, 153–165.
23 P. S. Addy, S. B. Erickson, J. S. Italia and A. Chatterjee, *Methods Mol. Biol.*, 2019, **2033**, 239–251.
24 H. Merten, J. V. Schaefer, F. Brandl, U. Zangemeister-Wittke and A. Plückthun, *Methods Mol. Biol.*, 2019, **2033**, 253–273.
25 F. Zappala and A. Tsourkas, *Methods Mol. Biol.*, 2019, **2033**, 275–286.
26 Y. Zhang, K. Y. Park, K. F. Suazo and M. D. Distefano, *Chem. Soc. Rev.*, 2018, **47**, 9106–9136.
27 B. Nilsson, T. Moks, B. Jansson, L. Abrahmsen, A. Elmblad, E. Holmgren, C. Henrichson, T. A. Jones and M. Uhlen, *Protein Eng.*, 1987, **1**, 107–113.
28 K. Nord, J. Nilsson, B. Nilsson, M. Uhlen and P. A. Nygren, *Protein Eng.*, 1995, **8**, 601–608.
29 J. M. Webster, R. Zhang, S. S. Gambhir, Z. Cheng and F. A. Syud, *ChemBioChem*, 2009, **10**, 1293–1296.
30 C. S. R. Gruning, E. A. Mirecka, A. N. Klein, E. Mandelkow, D. Willbold, S. F. Marino, M. Stoldt and W. Hoyer, *J. Biol. Chem.*, 2014, **289**, 23209–23218.
31 Affibody, **https://www.affibody.se**, (accessed 14 November, 2020).
32 S. Stahl, T. Graslund, A. E. Karlstrom, F. Y. Frejd, P. Nygren and J. Lofblom, *Trends Biotechnol.*, 2017, **35**, 691–712.
33 F. Y. Frejd and K. T. Kim, *Exp. Mol. Med.*, 2017, **49**, e306.
34 R. P. Baum, V. Prasad, D. Muller, C. Schuchardt, A. Orlova, A. Wennborg, V. Tolmachev and J. Feldwisch, *J. Nucl. Med.*, 2010, **51**, 892–897.
35 J. Sörensen, I. Velikyan, D. Sandberg, A. Wennborg, J. Feldwisch, V. Tolmachev, A. Orlova, M. Sandström, M. Lubberink, H. Olofsson, J. Carlsson and H. Lindman, *Theranostics*, 2016, **6**, 262–271.
36 M. A.-O. Oroujeni, S. A.-O. Rinne, A. A.-O. Vorobyeva, A. Loftenius, J. Feldwisch, P. Jonasson, V. Chernov, A. A.-O. Orlova, F. Y. Frejd and V. A.-O. Tolmachev, *Int. J. Mol. Sci.*, 2021, **22**(5), 2770.
37 J. Sorensen, I. Velikyan, D. Sandberg, A. Wennborg, J. Feldwisch, V. Tolmachev, A. Orlova, M. Sandstrom, M. Lubberink, H. Olofsson, J. Carlsson and H. Lindman, *Theranostics*, 2016, **6**, 262–271.
38 M. Sandstrom, K. Lindskog, I. Velikyan, A. Wennborg, J. Feldwisch, D. Sandberg, V. Tolmachev, A. Orlova, J. Sorensen, J. Carlsson, H. Lindman and M. Lubberink, *J. Nucl. Med.*, 2016, **57**, 867–871.
39 D. Sandberg, V. Tolmachev, I. Velikyan, H. Olofsson, A. Wennborg, J. Feldwisch, J. Carlsson, H. Lindman and J. Sorensen, *Eur. J. Nucl. Med. Mol. Imaging*, 2017, **44**, 1337–1346.
40 N. Zhou, C. Liu, X. Guo, Y. Xu, J. Gong, C. Qi, X. Zhang, M. Yang, H. Zhu, L. Shen and Z. Yang, *Eur. J. Nucl. Med. Mol. Imaging*, 2020, **48**, 161–175.
41 C. D. Martins, C. Da Pieve, T. A. Burley, R. Smith, D. M. Ciobota, L. Allott, K. J. Harrington, W. J. G. Oyen, G. Smith and G. Kramer-Marek, *Clin. Cancer Res.*, 2018, **24**, 1853–1865.
42 S. S. Rinne, C. Dahlsson Leitao, Z. Saleh-Nihad, B. Mitran, V. Tolmachev, S. Ståhl, J. Löfblom and A. Orlova, *Int. J. Mol. Sci.*, 2020, **21**(6), 1972.
43 A. L. de Souza, K. Marra, J. Gunn, K. S. Samkoe, P. J. Hoopes, J. Feldwisch, K. D. Paulsen and B. W. Pogue, *Mol. Imaging Biol.*, 2017, **19**, 41–48.
44 K. S. Samkoe, H. S. Sardar, J. Gunn, J. Feldwisch, K. Linos, E. Henderson, B. Pogue and K. Paulsen, *Proc. SPIE Int. Soc. Opt. Eng.*, 2019, 10862.
45 J. T. Elliott, A. V. Dsouza, K. Marra, B. W. Pogue, D. W. Roberts and K. D. Paulsen, *Biomed. Opt. Express*, 2016, **7**, 3280–3288.
46 K. S. Samkoe, H. S. Sardar, B. D. Bates, N. N. Tselepidakis, J. R. Gunn, K. A. Hoffer-Hawlik, J. Feldwisch, B. W. Pogue, K. D. Paulsen and E. R. Henderson, *J. Surg. Oncol.*, 2019, **119**, 1077–1086.
47 X. Su, K. Cheng, Y. Liu, X. Hu, S. Meng and Z. Cheng, *Amino Acids*, 2015, **47**, 1409–1419.
48 D. E. Gonzalez Trotter, X. Meng, P. McQuade, D. Rubins, M. Klimas, Z. Zeng, B. M. Connolly, P. J. Miller, S. S. O'Malley, S. A. Lin, K. L. Getty, L. Fayadat-Dilman, L. Liang, E. Wahlberg, O. Widmark, C. Ekblad, F. Y. Frejd, E. D. Hostetler and J. L. Evelhoch, *J. Nucl. Med.*, 2017, **58**, 1852–1857.
49 J. Garousi, H. Honarvar, K. G. Andersson, B. Mitran, A. Orlova, J. Buijs, J. Lofblom, F. Y. Frejd and V. Tolmachev, *Mol. Pharm.*, 2016, **13**, 3676–3687.
50 R. Bam, M. Laffey, K. Nottberg, P. S. Lown, B. J. Hackel and K. E. Wilson, *Bioconjugate Chem.*, 2019, **30**, 1677–1689.
51 R. Bam, P. S. Lown, L. A. Stern, K. Sharma, K. E. Wilson, G. R. Bean, A. M. Lutz, R. Paulmurugan, B. J. Hackel, J. Dahl and L. Abou-Elkacem, *Clin. Cancer Res.*, 2020, **26**, 2140–2150.
52 M. Altai, H. Liu, H. Ding, B. Mitran, P. H. Edqvist, V. Tolmachev, A. Orlova and T. Graslund, *J. Controlled Release*, 2018, **288**, 84–95.
53 Y. Ju, H. Zhang, J. Yu, S. Tong, N. Tian, Z. Wang, X. Wang, X. Su, X. Chu, J. Lin, Y. Ding, G. Li, F. Sheng and Y. Hou, *ACS Nano*, 2017, **11**, 9239–9248.

54 M. Satpathy, L. Wang, R. J. Zielinski, W. Qian, Y. A. Wang, A. M. Mohs, B. A. Kairdolf, X. Ji, J. Capala, M. Lipowska, S. Nie, H. Mao and L. Yang, *Theranostics*, 2019, **9**, 778–795.

55 A. Orlova, T. Z. Bass, S. S. Rinne, C. D. Leitao, M. Rosestedt, C. Atterby, L. Gudmundsdotter, F. Y. Frejd, J. Lofblom, V. Tolmachev and S. Stahl, *Mol. Pharmaceutics*, 2018, **15**, 3394–3403.

56 H. He, A. L. Nieminen and P. Xu, *Biomater. Sci.*, 2019, **7**, 5143–5149.

57 D. Jia, Y. Yang, F. Yuan, Q. Fan, F. Wang, Y. Huang, H. Song, P. Hu, R. Wang, G. Li, R. Liu and J. Li, *Int. J. Pharm.*, 2020, **586**, 119541.

58 Q. Fan, Z. Tao, H. Yang, Q. Shi, H. Wang, D. Jia, L. Wan, J. Zhang, J. Cheng and X. Lu, *J. Controlled Release*, 2019, **302**, 63–78.

59 Q. Shi, Z. Tao, H. Yang, Q. Fan, D. Wei, L. Wan and X. Lu, *Drug Delivery*, 2017, **24**, 1818–1830.

60 P. Jiang, L. Wang, B. Hou, J. Zhu, M. Zhou, J. Jiang, L. Wang, S. Chen, S. Zhu, J. Chen and L. Zhang, *Theranostics*, 2018, **8**, 3544–3558.

61 S. Zhu, J. Chen, Y. Xiong, S. Kamara, M. Gu, W. Tang, S. Chen, H. Dong, X. Xue, Z. M. Zheng and L. Zhang, *PLoS Pathog.*, 2020, **16**, e1008223.

62 D. R. Flower, *Biochem. J.*, 1996, **318**(Pt 1), 1–14.

63 M. Gebauer and A. Skerra, *Methods Enzymol.*, 2012, **503**, 157–188.

64 G. Beste, F. S. Schmidt, T. Stibora and A. Skerra, *Proc. Natl. Acad. Sci. U. S. A.*, 1999, **96**, 1898–1903.

65 C. Rothe and A. Skerra, *BioDrugs*, 2018, **32**, 233–243.

66 A. Azhar, E. Ahmad, Q. Zia, M. A. Rauf, M. Owais and G. M. Ashraf, *Int. J. Biol. Macromol.*, 2017, **102**, 630–641.

67 M. Gebauer and A. Skerra, *Curr. Opin. Biotechnol*, 2019, **60**, 230–241.

68 Pieris, **https://www.pieris.com/platform**, (accessed 14 November 2020).

69 A. G. T. T. Van Scheltinga, M. N. L. Hooge, M. Hinner, R. B. Verheijen, A. Allersdorfer, M. Hulsmeyer, W. B. Nagengast, C. P. Schroder, J. G. W. Kosterink and E. G. E. De Vries, *J. Nucl. Med.*, 2014, **55**, 665–671.

70 V. Albrecht, A. Richter, S. Pfeiffer, M. Gebauer, S. Lindner, E. Gieser, U. Schuller, C. Schichor, F. J. Gildehaus, P. Bartenstein, J. C. Tonn, A. Skerra and R. Glass, *Int. J. Cancer*, 2016, **138**, 1269–1280.

71 A. J. Reichert, G. Poxleitner, M. Dauner and A. Skerra, *Protein Eng., Des. Sel.*, 2015, **28**, 553–565.

72 C. Barinka, J. Ptacek, A. Richter, Z. Novakova, V. Morath and A. Skerra, *Protein Eng., Des. Sel.*, 2016, **29**, 105–115.

73 A. Richter and A. Skerra, *Biol. Chem.*, 2017, **398**, 39–55.

74 L. Friedrich, P. Kornberger, C. T. Mendler, G. Multhoff, M. Schwaiger and A. Skerra, *Biol. Chem.*, 2018, **399**, 235–252.

75 F. C. Deuschle, V. Morath, A. Schiefner, C. Brandt, S. Ballke, S. Reder, K. Steiger, M. Schwaiger, W. Weber and A. Skerra, *Theranostics*, 2020, **10**, 2172–2187.

76 M. Schlapschy, U. Binder, C. Börger, I. Theobald, K. Wachinger, S. Kisling, D. Haller and A. Skerra, *Protein Eng., Des. Sel.*, 2013, **26**, 489–501.

77 A. R. Sanchez-Paulete, S. Labiano, M. E. Rodriguez-Ruiz, A. Azpilikueta, I. Etxeberria, E. Bolaños, V. Lang, M. Rodriguez, M. A. Aznar, M. Jure-Kunkel and I. Melero, *Eur. J. Immunol.*, 2016, **46**, 513–522.

78 M. Hinner, R. B. Aiba, T. Jaquin, S. Berger, M. Durr, C. Schlosser, A. Allersdorfer, C. Rothe, L. Matis and S. Olwill, *Cancer Res.*, 2017, **77**, 3673.

79 M. J. Hinner, R. S. Bel Aiba, C. Schlosser, T. Jaquin, A. Allersdorfer, S. Berger, A. Wiedenmann, G. Matschiner, J. Schüler, U. Moebius, C. Rothe and S. A. Olwill, *Eur. J. Cancer*, 2016, **69**, S99.

80 M. J. Hinner, R. S. B. Aiba, T. J. Jaquin, S. Berger, M. C. Durr, C. Schlosser, A. Allersdorfer, A. Wiedenmann, G. Matschiner, J. Schuler, U. Moebius, C. Rothe, L. Matis and S. A. Olwill, *Clin. Cancer Res.*, 2019, **25**, 5878–5889.

81 S. Piha-Paul, J. Bendell, A. Tolcher, S. Hurvitz, A. Patnaik, R. Shroff, P. Pohlmann, M. Zettl, N. Hahn, A. Krishnamurthy, M. Duerr, J. Mei, K. Aviano, R. Yusuf, L. Matis, S. Olwill, I. Bruns and G. Ku, *J. ImmunoTher. Cancer*, 2020, **8**, A1.

82 M. J. Hinner, R.-S. B. Aiba, A. Wiedenmann, C. Schlosser, A. Allersdorfer, G. Matschiner, C. Rothe, U. Moebius, H. E. Kohrt and S. A. Olwill, *J. ImmunoTher. Cancer*, 2015, **3**, P187.

83 B. Bossenmaier, C. Schlosser, R. S. B. Aiba, C. Barthels, B. Weiche, T. Eichner, M. Yegres and S. Olwill, *Immunology*, 2019, **79**, 3268.

84 K. Mross, H. Richly, R. Fischer, D. Scharr, M. Buchert, A. Stern, H. Gille, L. P. Audoly and M. E. Scheulen, *PLoS One*, 2013, **8**, e83232.

85 H. Gille, M. Hulsmeyer, S. Trentmann, G. Matschiner, H. J. Christian, T. Meyer, A. Amirkhosravi, L. P. Audoly, A. M. Hohlbaum and A. Skerra, *Angiogenesis*, 2016, **19**, 79–94.

86 C. D. Dickinson, B. Veerapandian, X. P. Dai, R. C. Hamlin, N. H. Xuong, E. Ruoslahti and K. R. Ely, *J. Mol. Biol.*, 1994, **236**, 1079–1092.

87 P. G. Chandler and A. M. Buckle, *Cells*, 2020, **9**, 610.

88 A. Koide, C. W. Bailey, X. Huang and S. Koide, *J. Mol. Biol.*, 1998, **284**, 1141–1151.

89 Bristol-Myers Squibb, **https://www.bms.com/**, (accessed 14 November 2020).

90 A. Koide, J. Wojcik, R. N. Gilbreth, R. J. Hoey and S. S. Koide, *J. Mol. Biol.*, 2012, **415**, 393–405.

91 A. Natarajan and L. Abou-Elkacem, *Methods Mol. Biol.*, 2019, **2033**, 301–313.

92 F. Sha, G. Salzman, A. Gupta and S. Koide, *Protein Sci.*, 2017, **26**, 910–924.

93 A. W. Tolcher, C. Sweeney, K. P. Papadopoulos, A. Patnaik, E. G. Chiorean, A. C. Mita, K. K. Sankhala, E. Furfine, J. Gokemeijer and L. Iacono, *Clin. Cancer Res.*, 2011, **17**, 363–371.

94 L. Abouelkacem, K. E. Wilson, S. M. Johnson, S. M. Chowdhury, S. V. Bachawal, B. J. Hackel, L. Tian and J. K. Willmann, *Theranostics*, 2016, **6**, 1740–1752.

95 M. A. Kim, H. S. Yoon, S. H. Park, D. Y. Kim, A. Pyo, H. S. Kim, J. J. Min and Y. Hong, *PLoS One*, 2017, **12**, e0180786.

96 A. Pyo, S. H. You, H. Sik Kim, J. Young Kim, J. J. Min, D. Y. Kim and Y. Hong, *Bioorg. Med. Chem. Lett.*, 2020, **30**, 127262.

97 A. Natarajan, C. B. Patel, S. Ramakrishnan, P. S. Panesar, S. R. Long and S. S. Gambhir, *Clin. Cancer Res.*, 2019, **25**, 1774–1785.

98 S. Ramakrishnan, A. Natarajan, C. T. Chan, P. S. Panesar and S. S. Gambhir, *Protein Eng., Des. Sel.*, 2019, **32**, 231–240.

99 D. J. Donnelly, R. A. Smith, P. Morin, D. Lipovsek, J. Gokemeijer, D. Cohen, V. Lafont, T. Tran, E. L. Cole, M. Wright, J. Kim, A. Pena, D. Kukral, D. D. Dischino, P. Chow, J. Gan, O. Adelakun, X. T. Wang, K. Cao, D. Leung, S. J. Bonacorsi, Jr. and W. Hayes, *J. Nucl. Med.*, 2018, **59**, 529–535.

100 A. N. Niemeijer, D. Leung, M. C. Huisman, I. Bahce, O. S. Hoekstra, G. van Dongen, R. Boellaard, S. Du, W. Hayes, R. Smith, A. D. Windhorst, N. H. Hendrikse, A. Poot, D. J. Vugts, E. Thunnissen, P. Morin, D. Lipovsek, D. J. Donnelly, S. J. Bonacorsi, L. M. Velasquez, T. D. de Gruijl, E. F. Smit and A. J. de Langen, *Nat. Commun.*, 2018, **9**, 4664.

101 M. C. Huisman, A. N. Niemeijer, A. D. Windhorst, R. C. Schuit, D. Leung, W. Hayes, A. Poot, I. Bahce, T. Radonic, D. E. Oprea-Lager, O. S. Hoekstra, E. Thunnissen, N. H. Hendrikse, E. F. Smit, A. J. de Langen and R. Boellaard, *J. Nucl. Med.*, 2020, **61**, 1455–1460.

102 P. H. Nienhuis, I. F. Antunes, A. Glaudemans, M. Jalving, D. Leung, W. Noordzij, R. Slart, E. F. de Vries and G. A. P. Hospers, *J. Nucl. Med.*, 2021, **63**(6), 899–905.

103 D. Schiff, S. Kesari, J. de Groot, T. Mikkelsen, J. Drappatz, T. Coyle, L. Fichtel, B. Silver, I. Walters and D. Reardon, *Invest. New Drugs*, 2015, **33**, 247–253.

104 S. Aghaabdollahian, R. Ahangari Cohan, D. Norouzian, F. Davami, M. R. Asadi Karam, F. Torkashvand, G. Vaseghi, R. Moazzami and S. Latif Dizaji, *Sci. Rep.*, 2019, **9**, 2978.

105 X. Han, G. E. Cinay, Y. Zhao, Y. Guo, X. Zhang and P. Wang, *Mol. Ther.*, 2017, **25**, 2466–2476.

106 A. Gupta, J. Xu, S. Lee, S. T. Tsai, B. Zhou, K. Kurosawa, M. S. Werner, A. Koide, A. J. Ruthenburg, Y. Dou and S. Koide, *Nat. Chem. Biol.*, 2018, **14**, 895–900.

107 I. Khan, R. Spencer-Smith and J. P. O'Bryan, *Oncogene*, 2019, **38**, 2984–2993.

108 D. Lipovsek, I. M. Carvajal, A. Allentoff, A. Barros, J. Brailsford, Q. Cong, P. Z. Cotter, S. Gangwar, C. Hollander and V. Lafont, *Protein Eng., Des. Sel.*, 2018, **31**, 159–171.

109 A. R. Sirois, D. A. Deny, Y. Li, Y. D. Fall and S. J. Moore, *Biotechnol. Bioeng.*, 2020, **117**, 330–341.

110 P. Bork, *Proteins*, 1993, **17**, 363–374.

111 L. K. Mosavi, D. L. Minor, Jr. and Z. Y. Peng, *Proc. Natl. Acad. Sci. U. S. A.*, 2002, **99**, 16029–16034.

112 H. K. Binz, M. T. Stumpp, P. Forrer, P. Amstutz and A. Pluckthun, *J. Mol. Biol.*, 2003, **332**, 489–503.

113 Molecular Partners Allergan, **https://www.molecularpartners.com/**, (accessed 14 November 2020).

114 J. Schilling, J. Schoppe and A. Pluckthun, *J. Mol. Biol.*, 2013, **426**, 691–721.

115 M. Rasool, A. Malik, M. Hussain, K. A. Haq, K. Butt, M. A. B. Ashraf, M. I. Naseer, M. Asif, R. Shaikh, M. Z. Mustafa, Q. Alam, G. Rasool, W. Ahmad, A. Haque and M. A. Kamal, *Curr. Pharm. Des.*, 2017, **23**, 1610–1615.

116 Y. L. Boersma, *Methods Mol. Biol.*, 2018, **1798**, 307–327.

117 L. Kramer, M. Renko, J. Zavrsnik, D. Turk, M. A. Seeger, O. Vasiljeva, M. G. Grutter, V. Turk and B. Turk, *Theranostics*, 2017, **7**, 2806–2821.

118 D. L. Li, J. E. Tan, Y. Tian, S. Huang, P. H. Sun, M. Wang, Y. J. Han, H. S. Li, H. B. Wu, X. M. Zhang, Y. K. Xu and Q. S. Wang, *Biomaterials*, 2017, **147**, 86–98.

119 E. L. Guryev, N. Y. Shilyagina, A. B. Kostyuk, L. M. Sencha, I. V. Balalaeva, V. A. Vodeneev, O. M. Kutova, A. V. Lyubeshkin, R. I. Yakubovskaya, A. A. Pankratov, F. I. Ingel, T. S. Novik, S. M. Deyev, S. A. Ermilov and A. V. Zvyagin, *Toxicol. Sci*, 2019, **170**, 123–132.

120 S. Molavipordanjani, S. Khodashenas, S. M. Abedi, M. F. Moghadam, A. Mardanshahi and S. J. Hosseinimehr, *Eur. J. Pharm. Sci.*, 2020, **148**, 105312.

121 O. Bragina, V. Chernov, A. Schulga, E. Konovalova, E. Garbukov, A. Vorobyeva, A. Orlova, L. Tashireva, J. Sorensen, R. Zelchan, A. Medvedeva, S. Deyev and V. Tolmachev, *J. Nucl. Med.*, 2021, **63**(4), 528–535.

122 S. M. Deyev, A. Vorobyeva, A. Schulga, A. Abouzayed, T. Gunther, J. Garousi, E. Konovalova, H. Ding, T. Graslund, A. Orlova and V. Tolmachev, *Int. J. Biol. Macromol.*, 2020, **145**, 216–225.

123 A. Vorobyeva, E. Konovalova, T. Xu, A. Schulga, M. Altai, J. Garousi, S. S. Rinne, A. Orlova, V. Tolmachev and S. Deyev, *Int. J. Mol. Sci.*, 2020, **21**(9), 3310.

124 U. Fiedler, S. Ekawardhani, A. Cornelius, P. Gilboy, T. R. Bakker, I. Dolado, M. T. Stumpp and K. M. Dawson, *Oncotarget*, 2017, **8**, 98371–98383.

125 A. Azaro, J. Rodon, M. R. Middleton, R. D. Baird, R. Herrmann, U. Fiedler, J. Haunschild, M. Hauptle, F. Hermann and S. Schreiner, *J. Clin. Oncol.*, 2018, **36**, 2520.

126 R. D. Baird, C. Linossi, M. Middleton, S. Lord, A. Harris, J. Rodón, C. Zitt, U. Fiedler, K. M. Dawson, N. Leupin, M. T. Stumpp, A. Harstrick, A. Azaro, S. Fischer and A. Omlin, *J. Clin. Oncol.*, 2021, **39**, 145–154.

127 M. R. Middleton, A. Azaro, S. Kumar, P. Niedermann, J. Rodón, K. H. Herbschleb, J. Steiner, C. Zitt, D. Feurstein, S. Schreiner, D. Turner, K. Dawson, K. Tadjalli-Mehr, E. Baur, M. Stumpp, A. Harstrick, R. Baird and A. Omlin, *Ann. Oncol.*, 2016, **27**, vi115.

128 L. Rao, K. De Veirman, D. Giannico, I. Saltarella, V. Desantis, M. A. Frassanito, A. G. Solimando, D. Ribatti, M. Prete, A. Harstrick, U. Fiedler, H. De Raeve, V. Racanelli, K. Vanderkerken and A. Vacca, *Oncotarget*, 2018, **9**, 13366–13381.

129 F. Andres, L. Iamele, T. Meyer, J. C. Stuber, F. Kast, E. Gherardi, H. H. Niemann and A. Pluckthun, *J. Mol. Biol.*, 2019, **431**, 2020–2039.

130 A. Soto-Gamez, D. Chen, A. G. E. Nabuurs, W. J. Quax, M. Demaria and Y. L. Boersma, *Cancers*, 2020, **12**(2), 411.
131 J. R. H. Hanauer, V. Koch, U. M. Lauer and M. D. Muhlebach, *Mol. Ther. Oncolyt.*, 2019, **15**, 186–200.
132 E. L. Guryev, N. O. Volodina, N. Y. Shilyagina, S. V. Gudkov, I. V. Balalaeva, A. B. Volovetskiy, A. V. Lyubeshkin, A. V. Sen, S. A. Ermilov, V. A. Vodeneev, R. V. Petrov, A. V. Zvyagin, Z. I. Alferov and S. M. Deyev, *Proc. Natl. Acad. Sci. U. S. A.*, 2018, **115**, 9690–9695.
133 E. Siegler, S. Li, Y. J. Kim and P. Wang, *Hum. Gene Ther.*, 2017, **28**, 726–736.
134 A. Balakrishnan, A. Rajan, A. I. Salter, P. L. Kosasih, Q. Wu, J. Voutsinas, M. C. Jensen, A. Pluckthun and S. R. Riddell, *Clin. Cancer Res.*, 2019, **25**, 7506–7516.
135 G. S. Williams, B. Mistry, S. Guillard, J. C. Ulrichsen, A. M. Sandercock, J. Wang, A. Gonzalez-Munoz, J. Parmentier, C. Black, J. Soden, J. Freeth, J. Jovanovic, R. Leyland, R. S. Al-Lamki, A. J. Leishman, S. J. Rust, R. Stewart, L. Jermutus, J. R. Bradley, V. Bedian, V. Valge-Archer, R. Minter and R. W. Wilkinson, *Oncotarget*, 2016, **7**, 68278–68291.
136 S. Zhu, H. Darbon, K. Dyason, F. Verdonck and J. Tytgat, *FASEB J.*, 2003, **17**, 1765–1767.
137 B. Molesini, D. Treggiari, A. Dalbeni, P. Minuz and T. Pandolfini, *Br. J. Clin. Pharmacol.*, 2017, **83**, 63–70.
138 J. R. Kintzing and J. R. Cochran, *Curr. Opin. Chem. Biol.*, 2016, **34**, 143–150.
139 H. Kolmar, *FEBS J.*, 2008, **275**, 2684–2690.
140 O. Avrutina, *Adv. Exp. Med. Biol.*, 2016, **917**, 121–144.
141 AstraZeneca, **https://www.astrazeneca.com/**, (accessed 14 November).
142 Jazz, **https://www.jazzpharma.com/**, (accessed 14 November 2020).
143 Cyclogenix, **https://www.cyclogenix.com/**, (accessed 14 November 2020).
144 Ironwood, **https://ironwoodpharma.com/**, (accessed 14 November 2020).
145 C. Zhang, R. H. Kimura, L. Abouelkacem, J. Levi, L. Xu and S. S. Gambhir, *J. Nucl. Med.*, 2016, **57**, 1629–1634.
146 W. S. Tummers, R. H. Kimura, L. Abouelkacem, C. Beinat, A. L. Vahrmeijer, R. Swijnenburg, J. K. Willmann and S. S. Gambhir, *Clin. Cancer Res.*, 2018, **24**, 1667–1676.
147 R. H. Kimura, L. Wang, B. Shen, L. Huo, W. S. Tummers, F. V. Filipp, H. H. Guo, T. Haywood, L. Abouelkacem and L. Baratto, *Nat. Commun.*, 2019, **10**, 4673.
148 B. G. Lui, N. Salomon, J. Wustehube-Lausch, M. Daneschdar, H. U. Schmoldt, O. Tureci and U. Sahin, *Nat. Commun.*, 2020, **11**, 295.
149 J. W. Kim, F. V. Cochran and J. R. Cochran, *J. Am. Chem. Soc.*, 2015, **137**, 6–9.
150 N. Cox, J. R. Kintzing, M. Smith, G. A. Grant and J. R. Cochran, *Angew. Chem.*, 2016, **55**, 9894–9897.
151 N. V. Currier, S. E. Ackerman, J. R. Kintzing, R. Chen, M. F. Interrante, A. R. Steiner, A. K. Sato and J. R. Cochran, *Mol. Cancer Ther.*, 2016, **15**, 1291–1300.
152 S. Lal and C. Raffel, *Mol. Ther. Oncolyt.*, 2017, **7**, 57–66.
153 G. Cohen, S. R. Burks and J. A. Frank, *Toxins*, 2018, **10**, 496.
154 T. Park, K. A. Min, H. Cheong, C. Moon and M. C. Shin, *J. Drug Target*, 2019, **27**, 950–958.
155 J. Zhao, Y. Wang, X. Li, S. Gao, S. Liu, Y. Song, J. Wang, Y. Xiong, H. Ma and L. Jiang, *Contrast Media Mol. Imaging*, 2018, **2018**, 8439162.
156 J. Fidel, K. C. Kennedy, W. S. Dernell, S. Hansen, V. Wiss, M. R. Stroud, J. I. Molho, S. E. Knoblaugh, J. A. Meganck and J. M. Olson, *Cancer Res.*, 2015, **75**, 4283–4291.
157 Y. Jiang, E. J. Girard, F. Pakiam and E. J. Seibel, *J. Med. Imaging*, 2019, **6**, 025005.
158 C. G. Patil, D. G. Walker, D. M. Miller, P. Butte, B. Morrison, D. S. Kittle, S. J. Hansen, K. L. Nufer, K. A. Byrnes-Blake, M. Yamada, L. L. Lin, K. Pham, J. Perry, J. Parrish-Novak, L. Ishak, T. Prow, K. Black and A. N. Mamelak, *Neurosurgery*, 2019, **85**, E641–E649.
159 Dyax, **https://www.takeda.com/**, (accessed 14 November 2020).
160 T. Tian, J. Li, C. Xie, Y. Sun, H. Lei, X. Liu, J. Xia, J. Shi, L. Wang, W. Lu and C. Fan, *ACS Appl. Mater. Interfaces*, 2018, **10**, 3414–3420.
161 M. C. B. Schmidt, K. L. P. Morais, M. E. S. Almeida, A. Iqbal, M. B. Goldfeder and A. M. Chudzinski-Tavassi, *Cell Adhes. Migr.*, 2020, **14**, 129–138.
162 A. Sananes, I. Cohen, A. Shahar, A. Hockla, E. De Vita, A. K. Miller, E. S. Radisky and N. Papo, *J. Biol. Chem.*, 2018, **293**, 12663–12680.
163 L. K. Stadler, T. Hoffmann, D. C. Tomlinson, Q. Song, T. Lee, M. Busby, Y. Nyathi, E. Gendra, C. Tiede, K. Flanagan, S. J. Cockell, A. Wipat, C. Harwood, S. D. Wagner, M. A. Knowles, J. J. Davis, N. Keegan and P. K. Ferrigno, *Protein Eng., Des. Sel.*, 2011, **24**, 751–763.
164 Avacta Life Sciences, **https://avacta.com/**, (accessed 14 November 2020).
165 W. Wang, Y. Guo, C. Tiede, S. Chen, M. Kopytynski, Y. Kong, A. N. Kulak, D. C. Tomlinson, R. Chen and M. J. Mcpherson, *ACS Appl. Mater. Interfaces*, 2017, **9**, 15232–15244.
166 C. Tiede, R. Bedford, S. J. Heseltine, G. Smith, I. Wijetunga, R. Ross, D. AlQallaf, A. P. Roberts, A. Balls, A. Curd, R. E. Hughes, H. Martin, S. R. Needham, L. C. Zanetti-Domingues, Y. Sadigh, T. P. Peacock, A. A. Tang, N. Gibson, H. Kyle, G. W. Platt, N. Ingram, T. Taylor, L. P. Coletta, I. Manfield, M. Knowles, S. Bell, F. Esteves, A. Maqbool, R. K. Prasad, M. Drinkhill, R. S. Bon, V. Patel, S. A. Goodchild, M. Martin-Fernandez, R. J. Owens, J. E. Nettleship, M. E. Webb, M. Harrison, J. D. Lippiat, S. Ponnambalam, M. Peckham, A. Smith, P. K. Ferrigno, M. Johnson, M. J. McPherson and D. C. Tomlinson, *Elife*, 2017, **6**, e24903.
167 G. Behar, M. Bellinzoni, M. Maillasson, L. Paillard-Laurance, P. M. Alzari, X. He, B. Mouratou and F. Pecorari, *Protein Eng., Des. Sel.*, 2013, **26**, 267–275.
168 Affilogic, **https://www.affilogic.com/**, (accessed 14 November 2020).
169 M. Goux, G. Becker, H. Gorre, S. Dammicco, A. Desselle, D. Egrise, N. Leroi, F. Lallemand, M. A. Bahri and G. Doumont, *Bioconjugate Chem.*, 2017, **28**, 2361–2371.

170 J. Silverman, Q. Liu, A. Bakker, W. To, A. Duguay, B. M. Alba, R. Smith, A. Rivas, P. Li, H. Le, E. Whitehorn, K. W. Moore, C. Swimmer, V. Perlroth, M. Vogt, J. Kolkman and W. P. Stemmer, *Nat. Biotechnol.*, 2005, **23**, 1556–1561.

171 Amgen, **https://www.amgen.com/science**, (accessed 14 November 2020).

172 B. B. Kohnehrouz, A. Talischian, A. Dehnad and S. Nayeri, *Avicenna J Med Biotechnol*, 2017, **10**, 9–14.

173 Janseen, **https://www.janssen.com**, (accessed 14 November 2020).

174 S. Goldberg, R. Cardoso, T. Lin, T. Spinkadoms, D. Klein, S. Jacobs, V. Dudkin, G. L. Gilliland and K. Oneil, *Protein Eng., Des. Sel.*, 2016, **29**, 563–572.

175 S. M. Mahalingam, V. Y. Dudkin, S. Goldberg, D. Klein, F. Yi, S. Singhal, K. T. O'Neil and P. S. Low, *Bioconjug Chem*, 2017, **28**, 2865–2873.

176 S. Lorey, E. Fiedler, A. Kunert, J. Nerkamp, C. Lange, M. Fiedler, E. Bosse-Doenecke, M. Meysing, M. Gloser, C. Rundfeldt, U. Rauchhaus, I. Hanssgen, T. Gottler, A. Steuernagel, U. Fiedler and U. Haupts, *J. Biol. Chem.*, 2014, **289**, 8493–8507.

177 SCIL proteins, **https://www.scilproteins.com/**, (accessed 14 November 2020).

178 M. Kahl, F. Settele, P. Knick, U. Haupts and E. Bosse-Doenecke, *Protein Expr Purif*, 2018, **149**, 51–65.

179 J. N. Ahmad, J. Li, L. Biedermannova, M. Kuchař, H. Sipova, A. Semeradtova, J. Cerný, H. Petrokova, P. Mikulecký and J. Polinek, *Proteins*, 2012, **80**, 774–789.

180 H. Liu, S. Lindbo, H. Ding, S. Hober and T. Graslund, *Int. J. Oncol.*, 2019, **55**, 309–319.

181 E. von Witting, J. Garousi, S. Lindbo, A. Vorobyeva, M. Altai, M. Oroujeni, B. Mitran, A. Orlova, S. Hober and V. Tolmachev, *Eur. J. Pharm. Biopharm.*, 2019, **140**, 109–120.

182 J. Garousi, S. Lindbo, B. Mitran, J. Buijs, A. Vorobyeva, A. Orlova, V. Tolmachev and S. Hober, *Sci. Rep.*, 2017, **7**, 1–11.

183 D. A. Silva, B. E. Correia and E. Procko, *Methods Mol. Biol.*, 2016, **1414**, 285–304.

184 N. M. Barber, C. K. Y. Lau, L. Turner, G. Watson, S. Thrane, J. P. A. Lusingu, T. Lavstsen and M. K. Higgins, *mSphere*, 2021, **6**, e01081-20.

185 L. Holm and C. Sander, *Trends Biochem. Sci.*, 1995, **20**, 478–480.

186 X. Pan and T. Kortemme, *J. Biol. Chem.*, 2021, **296**, 100558.

187 A. Leaver-Fay, M. Tyka, S. M. Lewis, O. F. Lange, J. Thompson, R. Jacak, K. Kaufman, P. D. Renfrew, C. A. Smith, W. Sheffler, I. W. Davis, S. Cooper, A. Treuille, D. J. Mandell, F. Richter, Y. E. Ban, S. J. Fleishman, J. E. Corn, D. E. Kim, S. Lyskov, M. Berrondo, S. Mentzer, Z. Popović, J. J. Havranek, J. Karanicolas, R. Das, J. Meiler, T. Kortemme, J. J. Gray, B. Kuhlman, D. Baker and P. Bradley, *Methods Enzymol.*, 2011, **487**, 545–574.

188 B. E. Correia, J. T. Bates, R. J. Loomis, G. Baneyx, C. Carrico, J. G. Jardine, P. Rupert, C. Correnti, O. Kalyuzhniy, V. Vittal, M. J. Connell, E. Stevens, A. Schroeter, M. Chen, S. Macpherson, A. M. Serra, Y. Adachi, M. A. Holmes, Y. Li, R. E. Klevit, B. S. Graham, R. T. Wyatt, D. Baker, R. K. Strong, J. E. Crowe, Jr., P. R. Johnson and W. R. Schief, *Nature*, 2014, **507**, 201–206.

189 K. See, T. Kadonosono, K. Miyamoto, T. Tsubaki, Y. Ota, M. Katsumi, S. Ryo, K. Aida, M. Minegishi, T. Isozaki, T. Kuchimaru and S. Kizaka-Kondoh, *Sci. Rep.*, 2021, **11**, 22098.

190 C. M. Bryan, G. J. Rocklin, M. J. Bick, A. Ford, S. Majri-Morrison, A. V. Kroll, C. J. Miller, L. Carter, I. Goreshnik, A. Kang, F. DiMaio, K. V. Tarbell and D. Baker, *Proc. Natl. Acad. Sci. U. S. A.*, 2021, **118**, e2102164118.

191 J. Schymkowitz, J. Borg, F. Stricher, R. Nys, F. Rousseau and L. Serrano, *Nucleic Acids Res.*, 2005, **33**, W382–W388.

192 S. Yin, F. Ding and N. V. Dokholyan, *Nat. Methods*, 2007, **4**, 466–467.

193 M. A. Kruziki, S. Bhatnagar, D. R. Woldring, V. T. Duong and B. J. Hackel, *Chem. Biol.*, 2015, **22**, 946–956.

194 P. N. Pham, M. Huličiak, L. Biedermannová, J. Černý, T. Charnavets, G. Fuertes, Š. Herynek, L. Kolářová, P. Kolenko, J. Pavlíček, J. Zahradník, P. Mikulecky and B. Schneider, *Viruses*, 2021, **13**(2), 190.

195 M. A. Kruziki, V. Sarma and B. J. Hackel, *ACS Comb. Sci.*, 2018, **20**, 423–435.

196 V. Tolmachev and A. Orlova, *Cancers*, 2020, **12**(3), 651.

197 G. L. Verdine and L. D. Walensky, *Clin. Cancer Res.*, 2007, **13**, 7264–7270.

198 S. Grimm, E. Lundberg, F. Yu, S. Shibasaki, E. Vernet, M. Skogs, P. Nygren and T. Gräslund, *N. Biotechnol.*, 2010, **27**, 766–773.

199 S. Shibasaki, M. Karasaki, T. Gräslund, P. Nygren, H. Sano and T. Iwasaki, *AMB Express*, 2014, **4**, 82.

200 K. Kikuchi, M. Sugiura and T. Kimura, *Int. J. Pept.*, 2015, **2015**, 537508.

201 D. A. Richards, *Drug Discovery Today Technol.*, 2018, **30**, 35–46.

202 M. K. B. Ahmadi, S. A. Mohammadi, M. Makvandi, M. Mamouei, M. Rahmati, H. Dehghani and D. W. Wood, *Curr. Pharm. Biotechnol.*, 2021, **22**, 878–891.

203 J. Feldwisch, V. Tolmachev, C. Lendel, N. Herne, A. Sjöberg, B. Larsson, D. Rosik, E. Lindqvist, G. Fant, I. Höidén-Guthenberg, J. Galli, P. Jonasson and L. Abrahmsén, *J. Mol. Biol.*, 2010, **398**, 232–247.

204 B. J. Hackel, A. Sathirachinda and S. S. Gambhir, *Protein Eng., Des. Sel.*, 2012, **25**, 639–647.

205 A. R. Bilia, V. Piazzini, C. Guccione, L. Risaliti, M. Asprea, G. Capecchi and M. C. Bergonzi, *Planta Med.*, 2017, **83**, 366–381.

206 J. Feldwisch and V. Tolmachev, *Methods Mol. Biol.*, 2012, **899**, 103–126.

207 C. Eigenbrot, M. Ultsch, A. Dubnovitsky, L. Abrahmsén and T. Härd, *Proc. Natl. Acad. Sci. U. S. A.*, 2010, **107**, 15039–15044.

208 M. Gebauer, A. Schiefner, G. Matschiner and A. Skerra, *J. Mol. Biol.*, 2013, **425**, 780–802.

209 A. L. Main, T. S. Harvey, M. Baron, J. Boyd and I. D. Campbell, *Cell*, 1992, **71**, 671–678.

210 L. Chiche, A. Heitz and D. Le-Nguyen, Solution structure of the squash trypsin inhibitor EETI-II, **https://www.rcsb.org/structure/2IT7**, (accessed 2 October 2007).
211 A. Kohl, H. K. Binz, P. Forrer, M. T. Stumpp, A. Plückthun and M. G. Grütter, *Proc. Natl. Acad. Sci. U. S. A.*, 2003, **100**, 1700–1705.
212 A. Correa, S. Pacheco, A. E. Mechaly, G. Obal, G. Béhar, B. Mouratou, P. Oppezzo, P. M. Alzari and F. Pecorari, *PLoS One*, 2014, **9**, e97438.
213 S. D. Goldberg, R. M. Cardoso, T. Lin, T. Spinka-Doms, D. Klein, S. A. Jacobs, V. Dudkin, G. Gilliland and K. T. O'Neil, *Protein Eng., Des. Sel.*, 2016, **29**, 563–572.
214 B. Arnoux, A. Ducruix and T. Prangé, *Acta Crystallogr. D: Biol. Crystallogr.*, 2002, **58**, 1252–1254.
215 S. Jenko, I. Dolenc, G. Guncar, A. Dobersek, M. Podobnik and D. Turk, *J. Mol. Biol.*, 2003, **326**, 875–885.
216 D. Fass, S. Blacklow, P. S. Kim and J. M. Berger, *Nature*, 1997, **388**, 691–693.
217 R. Ramage, J. Green, T. W. Muir, O. M. Ogunjobi, S. Love and K. Shaw, *Biochem. J.*, 1994, **299**(Pt 1), 151–158.
218 H. Ebersbach, E. Fiedler, T. Scheuermann, M. Fiedler, M. T. Stubbs, C. Reimann, G. Proetzel, R. Rudolph and U. Fiedler, *J. Mol. Biol.*, 2007, **372**, 172–185.